Mathematisches Forschungsinstitut Oberwolfach

Report No. 04/2014

DOI: 10.4171/OWR/2014/04

Mixing, Transport and Coherent Structures

Organised by
Sanjeeva Balasuriya, Adelaide
George Haller, Zürich
Nicholas Ouellette, New Haven
Vered Rom-Kedar, Rehovot

26 January – 1 February 2014

Abstract. The subject of this workshop was coherent structures, which play a significant role in the transport and mixing of passive and active scalars in fluids on a wide range of spatial scales. Participants coming from diverse scientific communities such as experimental fluid flows, dynamical systems theory, computational mathematics and visualisation, reported on recent developments and open problems.

Mathematics Subject Classification (2010): 34xx, 35xx, 37xx, 76xx, 86xx.

Introduction by the Organisers

Coherent structures play a significant role in the *transport* and *mixing* of passive and active scalars in fluids. Such structures occur at spatial scales ranging from the geophysical to the nanofluidic. Understanding such structures is of considerable topical interest due to climate change concerns and biotechnological advances. Unambiguously identifying coherent structures is difficult due to many technical reasons, one of which is that viewing the time evolution of frozen-time information (e.g., contours of vorticity) does not in and of itself describe the transport of fluid particles. This has led to the development of a variety of ad hoc diagnostic tools for identifying coherent structures, algorithmically efficient methods for visualising such structures, and also theoretical descriptions that are valid under idealised conditions (e.g., assuming availability of infinite-time data sets). As these methods become increasingly sophisticated and efficient, questions regarding their true connection to transport in experimental and observational data remain.

Topics discussed at the workshop included:

Experimental and observational work. Substantial new experimental work has been done in fluid mixing, thanks in part to significantly improved digital imaging technology.

Mathematical tools in LCS detection and studying mixing. These include tools such as invariant manifolds, Kolmogorov-Arnol'd-Moser (KAM) surfaces, minimum flux curves/surfaces, minimum length-increase curves and transfer-operator decompositions. How do the insights obtained from the simplest models (periodic models with associated lobe dynamics, quasi-periodic or single-frequency dominated models) extend to theoretical results for more realistic situation of finite-time noisy data, possibly including stochastic effects?

Diagnostic tools for LCS detection and studying mixing. Examples include Finite-Time and Finite-Size Lyapunov Exponents, relative and absolute dispersion, complexity of fluid trajectories, and asymptotic ergodic methods applied to finite-time data. One of the main challenge in the field is to understand interrelationships between these diagnostic tools.

Computation and visualisation of LCS. These relate to the efficient computation of LCS based on either diagnostic or mathematical tools. Examples include efficient methods for scientific visualisation of LCS, parallel computations of Lagrangian trajectories, and handling challenging data sets.

We, the organizers, were pleased to see people from rather different areas interact with each other, stimulated by interesting talks, a very lively poster session and the special Oberwolfach spirit. We are sure that many coming scientific contributions to the theory and applications of mixing and transport will have their origin at this workshop.

Acknowledgement: The MFO and the workshop organizers would like to thank the National Science Foundation for supporting the participation of junior researchers in the workshop by the grant DMS-1049268, "US Junior Oberwolfach Fellows".

Workshop: Mixing, Transport and Coherent Structures

Table of Contents

Abstracts

Coherent structures in quasi-two-dimensional turbulence experiments

Robert E. Ecke

Quasi two-dimensional (2D) fluid flows represent an ideal testing ground for concepts of mixing, passive scalar transport, and nonlinear scale transfer processes. Experiments performed over the past decade on soap films [1, 4] and on stratified salt layers [2, 3, 5, 7, 8, 10, 11] have elucidated many important features of coherent structures. In addition to their important role in transport and mixing, coherent structures can also be related to turbulent cascade mechanisms [4, 10, 11]. For example, the mechanism in 2D turbulence [9] for the direct enstrophy cascade is the stretching of vortex patches in hyperbolic regions of the flow. This feature can be quantitatively captured by considering the spatially-resolved enstrophy flux [4] and demonstrating that enstrophy is preferentially forward in hyperbolic regions of the flow field. Fig. 1 shows a representative quasi two-dimensional flow, obtained using particle tracking velocimetry, where the tiny streaks are very short particle paths and the longer colored path is representative of a Lagrangian particle trajectory. Using the high-resolution (both space and time) velocity field,

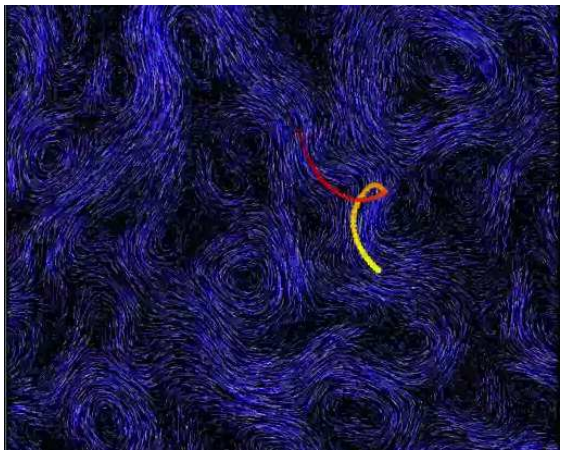

Figure 1. Streak image of quasi two-dimensional fluid flow. Also shown is a particle path color coded according to its speed.

one can compute an arbitrary number of Lagrangian trajectories of the flow. This approach can be used to investigate two particle dispersion in 2D turbulence [5]. These quasi two-dimensional experiments remain an important tool for elucidating the role of coherent structures, both Eulerian and Lagrangian, in real fluid flows. Although Eulerian coherent structure identification does not help elucidate energy transfer in the inverse energy cascade of 2D turbulence [6], recent results suggest that Lagrangian coherent structures may be more helpful in that context. There are certainly many more important concepts that can be tested and refined using quasi-2D experiments and, in cooperation with mathematicians, physicists and geophysicists, the future looks bright for new discoveries and insights.

References

[1] M.K. Rivera, P. Vorobieff and R.E. Ecke, *Turbulence in flowing soap films: velocity, vorticity, and thickness fields*, Phys. Rev. Lett. **81** (1998), 1417–1420.

[2] D. Rothstein, E. Henry and J.P. Gollub, *Persistent patterns in transient chaotic fluid mixing*, Nature **401** (1999), 770–772.

[3] G.A. Voth, G. Haller and J.P. Gollub, *Experimental measurements of stretching fields in fluid mixing*, Phys. Rev. Lett. **88** (2002), 254501.

[4] M.K. Rivera, W.B. Daniel, S.Y. Chen and R.E. Ecke, *Energy and enstrophy transfer in decaying two-dimensional turbulence*, Phys. Rev. Lett. **90** (2003), 104502.

[5] M.K. Rivera and R.E. Ecke, *Pair dispersion and doubling time statistics in two-dimensional turbulence*, Phys. Rev. Lett. **95** (2005), 194503.

[6] S.Y. Chen, R.E. Ecke, G.L. Eyink, M.K. Rivera, M.P. Wan and Z. Xiao, *Physical mechanism of the two-dimensional inverse energy cascade*, Phys. Rev. Lett. **96** (2006), 084502.

[7] M.J. Twardos, P.E. Arratia, M.K. Rivera, G. A. Voth, J. P. Gollub and R. E. Ecke, *Stretching fields and mixing near the transition to nonperiodic two-dimensional flow*, Phys. Rev. E **77** (2008), 056315.

[8] D.H. Kelley and N.T. Ouellette, *Separating stretching from folding in fluid mixing*, Nature Physics **11** (2011), 477–480.

[9] G. Boffetta and R.E. Ecke, *Two Dimensional Turbulence*, Annu. Rev. Fluid Mech. **44** (2012), 427–451.

[10] D.H. Kelley, M.R. Allshouse and N.T. Ouellette, *Lagrangian coherent structures separate dynamically distinct regions in fluid flows*, Phys. Rev. E **88** (2013), 013017.

[11] Y. Liao and N.T. Ouellette, *Spatial structure of spectral transport in two-dimensional flow*, J. Fluid Mech. **725** (2013), 281–298.

Ocean mixing and dispersion: Combining theory and observations

Hezi Gildor

Studying ocean mixing and dispersion is difficult because the processes are intermittent in time, highly nonlinear, and very inhomogeneous in space. Moreover, these processes span a wide range of spatial and temporal scales, and all these scales interact with all other scales in a non-linear manner making it hard to evaluate the importance of processes since even a weak perturbation can produce significant changes. The so-called "submesoscale" processes, composing of motions on a scale of a few kilometers, form a gap in both observations and understanding of processes with spatial scale between few tens of km (which can be studied using satellites data) and very fine-scale (centimeters to meters turbulent motions) which can be studied using microstructure turbulence profilers.

Recent advances in ocean observing systems enable us to reconstruct quasi-synoptic maps of ocean surface velocity field, over large areas and at high spatial (hundreds of meter) and temporal (30 min) resolutions. These surface current observations allow the computation of Lagrangian trajectories of many virtual particles. Based on these trajectories, one can compute various measures for mixing (such as absolute and relative dispersion) and identified Lagrangian Coherent Structures (LCS) using various methods (such as Finite-Time and Finite-Size Lyapunov Exponents).

I will present few studies based on surface currents observed by High-Frequency (HF) radar for current measurements in the Gulf of Eilat (northern Red Sea) and on simple toy models.

Evidence for submesoscale barriers to horizontal mixing [3]: Using the HF radar dataset of surface currents that we collected at high spatial (300 m) and temporal (30 min) resolutions, we demonstrate experimentally the existence of temporary barriers to mixing. This has important implications for the dispersion of pollutants, nutrients, larvae, etc., and therefore for a wide range of predictions. We were able to also verify the existence of these barriers by aerial-photographs. In addition, the dependency of the absolute dispersion on time is not as expected from diffusion-like behavior and is different on the two sides of the barriers.

Deducing an upper bound to the horizontal eddy diffusivity using a stochastic Lagrangian model [2]: We present a method for estimating the upper bound of the horizontal eddy diffusivity using a non-stationary Lagrangian stochastic model. First, we identify a mixing barrier using a priori evidence (e.g., aerial photographs or satellite imagery) and using a Lagrangian diagnostic calculated from observed or modeled spatially non-trivial, time-dependent velocities [for instance, the relative dispersion (RD)]. Second, we add a stochastic component to the observed velocity field. The stochastic component represents sub-grid stochastic diffusion and its mean magnitude is related to the eddy diffusivity. The RD of Lagrangian trajectories is computed for increasing values of the eddy diffusivity until the mixing barrier is no longer present. The value at which the mixing barrier disappears provides a dynamical estimate of the upper bound of the eddy diffusivity. The erosion of the mixing barrier is visually observed in numerical simulations, and is quantified by computing the kurtosis of the RD at each value of the eddy diffusivity. We demonstrate our method using the double gyre circulation model and apply it to high frequency radar observations of surface currents in the Gulf of Eilat.

When complexity leads to simplicity: Ocean surface mixing simplified by vertical convection [1]: In many applications, for example, when studying submesoscale (100 m – 20 km) dynamics, the flow field in the ocean is three dimensional. The effect of weak vertical motion on the dynamics of materials that are limited to move on the ocean surface is an unresolved problem with important environmental and ecological implications (e.g., oil spills and larvae dispersion). We investigate this effect by introducing into the classical horizontal time-periodic double-gyre model vertical motion associated with diurnal convection. The classical model produces chaotic advection on the surface. In contrast, the weak vertical motion simplifies this chaotic surface mixing pattern for a wide range of parameters. Melnikov analysis is employed to demonstrate that these conclusions are general and may be applicable to realistic cases. This counter intuitive result that the very weak nocturnal convection simplifies ocean surface mixing has significant outcomes.

References

[1] R. Aharon, V. Rom-Kedar and H. Gildor, *When complexity leads to simplicity: Ocean surface mixing simplified by vertical convection*, Phys. Fluids **24** (2012), 056603.

[2] D. Carlson, E. Fredj, H. Gildor and V. Rom-Kedar, *Deducing an upper bound to the horizontal eddy diffusivity using a stochastic Lagrangian model*, Environ. Fluid Mech. **10** (2010), 499–520.

[3] H. Gildor, E. Fredj, J. Steinbuck and S. Monismith, *Evidence for submesoscale barriers to horizontal mixing in the ocean from current measurements and aerial-photographs*, J. Phys. Oceanogr. **39** (2009), 1975–1983.

Optimal stirring for maximal mixing

Charles R. Doering

We address the challenge of optimal incompressible stirring to mix an initially inhomogeneous distribution of passive tracers. As a measure for mixing we adopt the H^{-1} norm of the scalar fluctuation field. This 'mix-norm' is equivalent to (the square root of) the variance of a low-pass filtered image of the tracer concentration field, and is a useful gauge even in the absence of molecular diffusion. This mix-norm's vanishing as time progresses is evidence of the stirring flow's mixing property in the sense of ergodic theory. For the case of a periodic spatial domain with a prescribed instantaneous energy or power budget for the stirring, we determine the flow field that instantaneously maximizes the decay of the mix norm, i.e., the instantaneous optimal stirring—when such a flow exists. When no such 'steepest descent' stirring exists, we determine the flow that maximizes that rate of increase of the rate of decrease of the norm. This local-in-time stirring strategy is implemented computationally on a benchmark problem and compared to an optimal control approach utilizing a restricted set of flows.

References

[1] Z. Lin, J.-L. Thiffeaul and C.R. Doering. *Optimal stirring strategies for passive scalar mixing*, J. Fluid Mech. **675** (2011), 465–476.

[2] E. Lunasin, Z. Lin, A. Novikov, A. Mazzucato and C.R. Doering. *Optimal mixing and optimal stirring for fixed energy, fixed power, or fixed palenstrophy flows*, J. Math. Phys. **53** (2012), 115611.

Mixing, manifolds and reaction fronts in laminar flows

Tom Solomon

We are conducting experiments that investigate the effects of mixing on reactions in fluid flows. Studies of these *advection-reaction-diffusion* (ARD) processes benefit significantly from recent advancements in theories of chaotic advection. In particular, analysis techniques for mixing based on manifolds and finite-time Lyapunov exponents can be adapted to the case of reacting impurities. This is a subject with significant practical applications to a wide range of ARD systems, including microfluidic chemical and biological devices, cellular-scale processes in

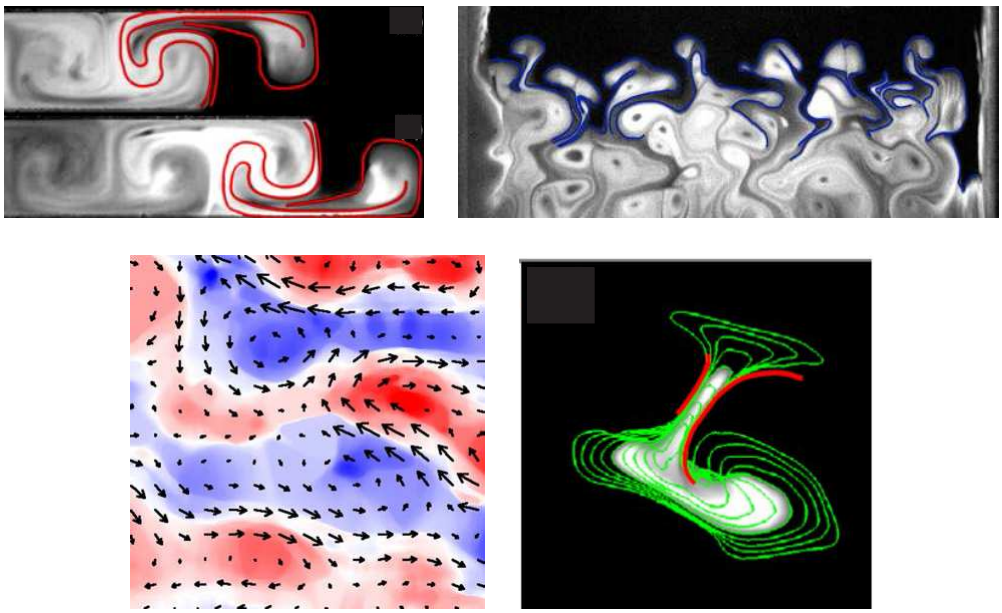

FIGURE 1. Top left: BIMs (in red) act as local barriers to front in an oscillating vortex chain. Top right: BIMs (in blue) pin reactions fronts in a disordered flow with an imposed wind (blowing downward). Bottom: spatially-random flow and BIMs (in red) that block an evolving front (green contour lines).

biological systems, oceanic ecosystems (such as plankton blooms), ignition fronts in supernova explosions, and the spreading of a disease in a moving population.

To understand how reaction fronts propagate in ARD systems, we have adapted manifold techniques developed to analyze chaotic mixing. We define *burning invariant manifolds* (BIMs) that act as barriers to propagating fronts, similar to invariant manifolds that block passive mixing. However, BIMs are one-way barriers, blocking fronts that propagate in one direction but not the other. We use the BIM approach to identify barriers to front propagation in vortex chain flows and spatially-disordered flows, as well as pinning of fronts in vortex chains and disordered flows with imposed winds, see Fig. 1.

Coherent structures and transport in three-dimensional unsteady flows

MICHEL SPEETJENS

(joint work with Neehar Moharana, Ruben Trieling, Herman Clercx)

Scalar transport (additives, chemical species, heat) in 3D deterministic flows is key to a wide variety of industrial and natural fluid flows of size extending from microns to hundreds of kilometers. Fluid advection plays a central role in scalar transport and is an essentially Lagrangian process. This advances a Lagrangian perspective based on the properties of fluid trajectories as a natural way for its description. Mass and momentum conservation "organise" these trajectories into

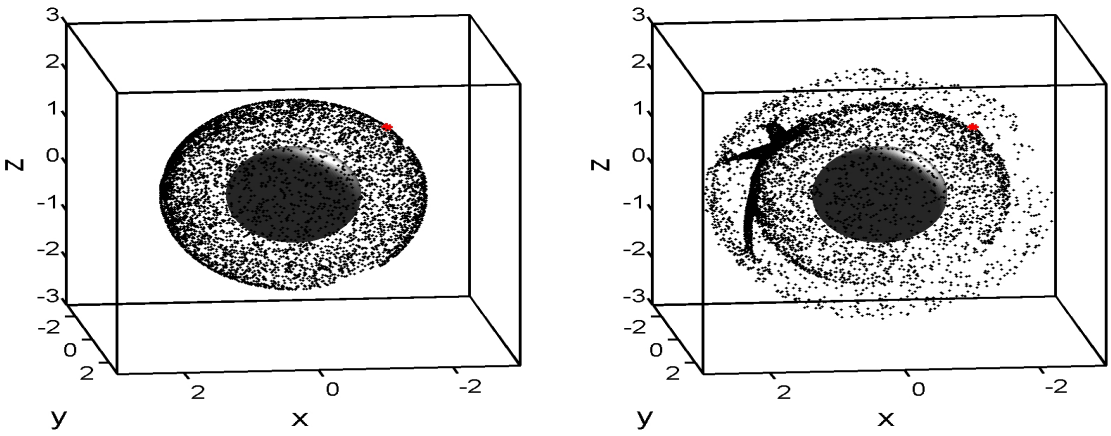

FIGURE 1. 3D Poincaré section of unperturbed (left) and perturbed (right) time-periodic sphere-driven flow [3].

coherent structures that geometrically determine the transport properties. 3D unsteady flows admit the highest dynamic freedom and, in consequence, exhibit the greatest diversity in coherent structures and richness in transport characteristics.

The present study concerns 3D time-periodic flows, where coherent structures emerge as periodically-recurring material entities in the associated stroboscopic maps. A class of structures of great (practical) relevance are invariant closed surfaces, with tori and spheroids as basic kinds. Studies in literature generally concern the former; investigations on the latter are rare. The different topology (spheroids/tori are singly/doubly-connected) implies fundamentally different dynamics [1]. Tori accommodate windings of trajectories and respond to perturbations as per 3D counterparts of the well-known KAM/Poincaré-Birkhoff theorems [2]. Spheroids accommodate 2D (chaotic) Hamiltonian dynamics [3]. Simulation of their response to weak fluid inertia in an interior flow in a finite cylinder revealed remarkable behaviour: formation of intricate coherent structures by merger of thin shells and tubes [1, 4]. A recent study exposed essentially similar behaviour in an exterior flow driven by a rotating sphere and subjected to an artificial perturbation [3]. This demonstrated the universal nature of the observed response scenario.

The 3D time-periodic sphere flow is composed of step-wise reorientations of a steady base flow $\bar{\mathbf{u}} = \bar{\mathbf{u}}_0 + \bar{\mathbf{u}}'$, with $\bar{\mathbf{u}}_0$ a Stokes flow and $\bar{\mathbf{u}}'$ a divergence-free perturbation $\bar{\mathbf{u}}'$, driven by rotation of the sphere about the z-axis.

Perturbation can trigger invariant spheres with 2D Hamiltonian dynamics ("2D mode") or structures as in the above-mentioned cylinder flow [3]. Former and latter are demonstrated in Fig. 1 by the Poincaré section (black markers) of a single tracer (released at the red marker) in a 2-step flow (rotation about about z and x-axes).

The formation of shells and tubes upon perturbation is the result of the so-called averaging that happens for Lagrangian motion with "slow" and "fast" components [5]. Perturbation of chaotic regions within invariant spheres results in significant motion parallel to said spheres (two "fast" components) and weak radial motion

(one "slow" component). The "slow" component is on average constant and thus to good approximation acts as a constant of motion ("adiabatic invariant" [5]).

Hence the spheroidal shells. This averaging process breaks down near elliptic islands within the original invariant surfaces due to essentially different (local) dynamics: one "fast" and two "slow" components parallel and transverse, respectively, to the original closed orbits. The "slow" components, rather than becoming individual adiabatic invariants, cause one (local) adiabatic invariant[1] with toroidal level sets defined by coalescence of elliptic orbits on adjacent spheres [6]. Hence the tubes.

Emergence of shells and tubes and their interaction is inextricably linked to periodic entities. Restriction to invariant spheres in the "2D mode" results in "periodic lines", i.e. material curves that consist of individual periodic points of either elliptic or hyperbolic type. The former are the centers of elliptic islands; the latter are the origin of pairs of stable-unstable 1D manifolds that densely fill the chaotic regions. Perturbation causes hyperbolic and elliptic segments of periodic lines to give way to isolated periodic points in 3D of focus-type and node-type, respectively [2]. The 1D/2D manifold pairs of nodes, consistent with the response of the chaotic regions associated with the underlying hyperbolic points, proliferate within shells. This is demonstrated in Fig. 2 by the 1D unstable (red) and 2D stable (green) manifold of a period-3 node. The 2D manifolds of foci also proliferate within shells (not shown) due to the dominance of shell formation outside the original elliptic islands. The 1D manifolds of foci, on the other hand, are an exception. Elliptic segments of periodic lines are unperturbed limits of foci and corresponding 1D manifolds; the aforementioned correlation between elliptic segments and foci extends to the associated 1D manifolds of the latter. Thus the 1D manifolds become the centers of the tubes that emanate from the perturbed elliptic islands. This is demonstrated in Fig. 2 by the 1D unstable manifolds (blue) of a cluster of period-3 foci (red markers), which run through the tubes.

The manifold behaviour enables tube-shell merger in two distinct ways. First, shells and tubes centre on the 2D and 1D manifolds, respectively, of the foci. This happens at the inner shell in Fig. 2 (2D manifold not shown) and is in accordance with [2]. Second, manifolds of nodes obstruct radial proliferation of the 1D manifold of the foci, causing deflection into a shell (outer shell in Fig. 2). Important to note is the absence of foci here, signifying that an essentially different mechanism than at the inner shell is at play, namely the property that 1D/2D manifolds cannot intersect—and thus cross—2D manifolds of the same type.

The behaviour of spheroids, despite fundamental differences with tori, has certain parallels with the latter. Chaotic sections on spheroids survive as shells in a way reminiscent of KAM tori emanating from perturbed non-resonant tori. Elliptic islands on spheroids give way to new structures (i.e. tubes) by locally interrupting shell formation in a manner akin to resonant tori disintegrating into clusters of

[1]Local in the sense of existing only in the direct vicinity of the original elliptic islands.

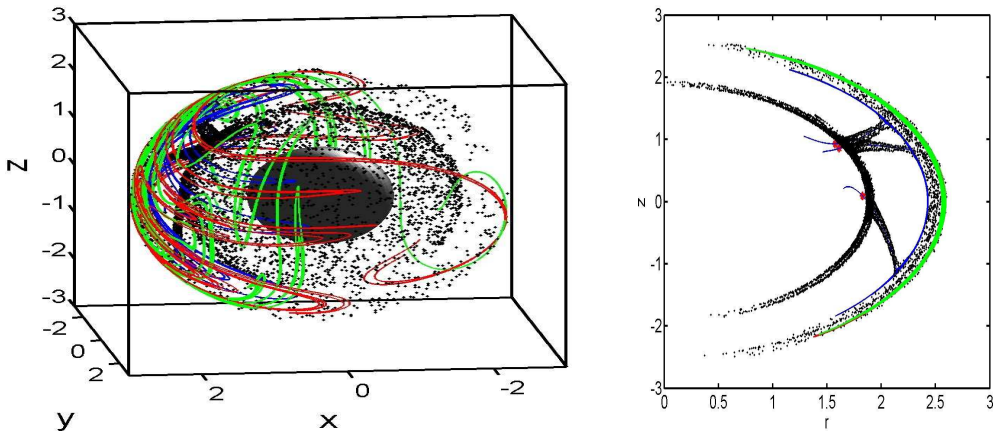

FIGURE 2. Manifold dynamics in perturbed sphere-driven flow [3].

higher-order tubes embedded in local chaotic zones. Hence, (non-)chaotic sectors on spheroids are in this sense counterparts to (non-)resonant tori.

Further studies to unravel the response of invariant spheroids to perturbation and the resulting formation of intricate coherent structures are in progress. Moreover, experimental studies to validate the observed phenomena are underway.

REFERENCES

[1] M. F. M. Speetjens, H. J. H. Clercx, G. J. F. van Heijst, *Inertia-induced coherent structures in a time-periodic viscous mixing flow*, Phys. Fluids **18** (2006), 083603.
[2] I. Mezić, *Break-up of invariant surfaces in action-angle-angle maps and flows*, Physica D **154** (2001), 51–67.
[3] N. R. Moharana, M. F. M. Speetjens, R. R. Trieling, H. J. H. Clercx, *Three-dimensional Lagrangian transport phenomena in unsteady laminar flows driven by a rotating sphere*, Phys. Fluids **25** (2013), 093602.
[4] Z. Pouransari, M. F. M. Speetjens, H. J. H. Clercx, *Formation of coherent structures by fluid inertia in three-dimensional laminar flows*, J. Fluid Mech. **654** (2010), 5.
[5] V.I. Arnol'd, *Mathematical Methods of Classical Mechanics*, Springer, 1978.
[6] J. H. E. Cartwright, M. Feingold, O. Piro, *Chaotic advection in three-dimensional unsteady incompressible laminar flow*, J. Fluid Mech. **316** (1996), 259.

Observations of Lagrangian transport in the Adriatic Sea from GPS-tracked surface drifters

DANIEL CARLSON

(joint work with Lorenzo Corgnati,Carlo Mantovani, Marcello Magaldi, Annalisa Griffa, Enrico Zambianchi, Pierre M. Poulain)

While most large-scale studies of population connectivity use numerical ocean model output to compute statistics of thousands of virtual particles, large uncertainties persist as models have limited spatial resolution and often do not reproduce observed ocean variability. Furthermore, scale-dependent dispersion on the surface ocean remains an important open subject in physical oceanography. Lagrangian

observations from surface drifters come with their own set of problems, most notably limited numbers, sampling bias, finite lifetime, and position uncertainties from wind and wave effects. Despite their limitations, surface drifter trajectories provide important observations of surface ocean transport.

Twenty six GPS-tracked surface tracked drifters were deployed in the central Adriatic Sea in May 2013 to investigate surface transport and to identify Lagrangrian pathways. Or particular interest are transit times between the Italian peninsula and the east coast (Croatia and Albania) as well as transit times between the network of marine protected areas (MPAs) in the Adriatic Sea.Preliminary results reveal transit times between MPAs in the central and southern Adriatic that vary from a few days to a few months. None of the drifters released in this experiment reached the Albanian coast. The drifters exited the Adriatic Sea by the end of July 2013 with several traveling to the Ionian Sea.

The drifter trajectories observed were determined by ambient environmental conditions (currents, winds, waves, stratification, etc.). Therefore, to determine the degree to which the present results can be extrapolated, the May 2013 drifter trajectories will be compared to a historical dataset of over 300 drifter trajectories in the Adriatic Sea. Additionally, the atmospheric and oceanographic conditions during the May 2013 experiment will be compared to climatological conditions. Future work will include tracking of thousands of virtual particles using output from a Regional Ocean Modeling System (ROMS) simulation of the Adriatic Sea during the same time period.

Lagrangian descriptors and their applications to geophysical flows

Ana M. Mancho

(joint work with Stephen Wiggins, Jezabel Curbelo, Carolina Mendoza)

We report new techniques, which we refer to as *Lagrangian descriptors* (LD), for revealing geometrical structures in phase space that are valid for aperiodically time dependent dynamical systems [1]. These are based on the integration, for a finite time, along trajectories of an intrinsic bounded, positive geometrical and/or physical property of the trajectory itself. Let $|\mathcal{F}(\mathbf{x})|$ denote this property, let $\mathbf{x}(t)$ be a trajectory satisfying $\mathbf{x}(t^*) = \mathbf{x}^*$ and defined on the time interval $(t^*-\tau, t^*+\tau)$. Then $|\mathcal{F}(\mathbf{x}(t))|$ is a scalar valued function of t that depends parametrically on $\mathbf{x}^*$ and t^*. We can consider its L^γ norm:

$$M(\mathbf{x}^*, t^*)_{\mathbf{v},\tau} = \left(\int_{t^*-\tau}^{t^*+\tau} |\mathcal{F}(\mathbf{x}(t))|^\gamma \, \mathrm{d}t \right)^\beta ,$$

where $\beta = 1$ if $\gamma \leq 1$ and $\beta = 1/\gamma$ if $\gamma > 1$. Here $|\mathcal{F}(\mathbf{x}(t))|$ can be the modulus of the velocity, or the modulus of the acceleration, or the modulus of the time derivative of the acceleration. LD highlight invariant manifolds by means of abrupt changes across the manifolds that denote lack of regularity of the underlying function over these lines. The visualization of this effect requires long enough integration times τ. Heuristic arguments supporting the performance of

LD are given in [1, 3, 7, 2]. Additionally, analytical arguments based on explicit calculations on a benchmark problem having a hyperbolic fixed point with stable and unstable manifolds are given in [1]. Computations of LD for an explicitly three dimensional, aperiodically time-dependent vector field, the time dependent Hill's spherical vortex [1], confirms a full agreement between the features provided by LD and those obtained from the direct manifold calculation [4]. LD are also a useful tool for analyzing elliptic regions in time dependent flows (see discussions in [1, 3, 2]).

Lagrangian descriptors have been applied to geophysical flows defined as data sets such as the Antarctic polar vortex in the southern stratosphere [5, 6]. Comparisons of the performance of LD with both finite time Lyapunov exponents (FTLEs) and finite size Lyapunov exponents (FSLEs) in this geophysical flow confirm a better performance of LD. The maps of LD systematically display sharper plots that facilitate the identification of Lagrangian coherent structures and lobe dynamics. For instance in [5] routes of transport that cross the Antarctic polar jet are identified. This would not have been possible using FTLE since they provide a blurred pattern, full of spurious structures. In [5] LD features provide a picture where Rossby wave breaking evidence is found in the interior of the vortex, while these features are unnoticed with other Lagrangian approaches. A full comparison of the performance of LD versus FTLE and other Lagrangian techniques, such as finite time averages, is reported in [1].

Frame invariance is related to how LD perform in different coordinate systems. Under coordinate transformations the results obtained from LD transform according to the manner in which the type of invariant objects that they are expected to recover transform. However, we note that in general these invariant objects are not preserved under arbitrary coordinate transformations, for instance they are not preserved for those time dependent transformations in which a new reference system is built by subtracting from the old coordinates one of its trajectories. A thorough discussion of these issues may be found in [7]. If the coordinates of a dynamical system are transformed, the values of the LD at specific points of space will certainly change with the reference frame, but the edges at which LD changes abruptly—which are the features containing the Lagrangian information—are transformed with the change of coordinates in the same manner in which the manifolds themselves are transformed.

References

[1] A.M. Mancho, S. Wiggins, J. Curbelo and C. Mendoza, *Lagrangian Descriptors: A Method for Revealing Phase Space Structures of General Time Dependent Dynamical Systems*, Commun. Nonlinear Sci. Numer. Simulat. **18** (2013), 3530–3557.

[2] J.A.J. Madrid and A.M. Mancho, *Distinguished trajectories in time dependent vector fields*, Chaos **19** (2009), 013111.

[3] C. Mendoza and A.M. Mancho, *Hidden Geometry of Ocean Flows*, Phys. Rev. Lett. **105** (2010), 038501.

[4] M. Branicki and S. Wiggins. *An adaptive method for computing invariant manifolds in non-autonomous, three-dimensional dynamical systems*, Physica D **238** (2009), 1625–1657.

[5] A. de la Cámara, A.M. Mancho, K. Ide, E. Serrano and C.R. Mechoso, *Routes of transport across the Antarctic polar vortex in the southern spring*, J. Atmospheric Sci. **69** (2012), 753–767.

[6] A. de la Cámara, R. Mechoso, A.M. Mancho, E. Serrano and K. Ide. *Quasi-horizontal transport within the Antarctic polar night vortex: Rossby wave breaking evidence and Lagrangian structures*, J. Atmospheric Sci. **70** (2013), 2982–3001.

[7] C. Mendoza and A.M. Mancho, *The Lagrangian description of aperiodic flows: a case study of the Kuroshio Current*, Nonlin. Processes Geophys. **19** (2012), 449–472.

Reacting flows and turnstiles

John R. Mahoney
(joint work with Kevin A. Mitchell)

In this work, we analyze the interplay between front propagation and the canonical turnstile structure of dynamical systems theory. The result is our modified structure, the *burnstile*, which accounts for both dynamical contributions. We show how many features carry over naturally, and several new ones emerge. In particular, it is necessary to account for the one-sided nature of the new *burning invariant manifolds*, and their ability to form swallowtails.

We frame this work by posing a toy problem. Imagine an ocean bay where the flow near the bay mouth is well-modeled by a separatrix under tidal (periodic) driving. This of course leads to a turnstile (Fig. 1(left)) in the fluid dynamics that describes the transport of fluid in and out of the bay [1]. Now, consider a hypothetical algae bloom just outside the bay mouth that threatens to invade the bay, causing ecological harm. We wish to prevent this invasion by applying algaecide to the ocean surface. Suppose that the algaecide is applied once every tidal cycle, and that it is perfectly effective and then immediately degrades.

Our motivating question is: Where should we apply this algaecide in order to most effectively prevent invasion?

We illustrate the result of three protocols in Fig. 1(middle). The first column is a control, showing the unchallenged progress of algae. Notice that by the third cycle, it has penetrated the turnstile and will shortly overwhelm the whole bay. In the first attempt we treat a rectangular strip that spans the channel. This is clearly insufficient. The second attempt makes use of the underlying turnstile structure, targeting the E_0 lobe. This is a step in the right direction, but notice that at $2T$ the algae has grown outward to occupy a "fattened" E_0 lobe. The algae missed by this treatment then goes on to invade, resulting in little improvement from the control. The last treatment is applied to a lobe that has been "fattened" by an amount v_0T. This is closer to complete, however the treated region does not properly account for the shape of the algae. Due to the expanding algae dynamic, even this small leak results in eventual failure.

The answer lies in considering the invariant manifolds of the joint dynamics—the so-called *burning invariant manifolds (BIMs)* [2, 3, 4, 5]. By modifying the set-based definitions of lobes to naturally account for this one-to-many map (small algae blobs to larger ones), we find that the modified lobes are bounded by BIMs.

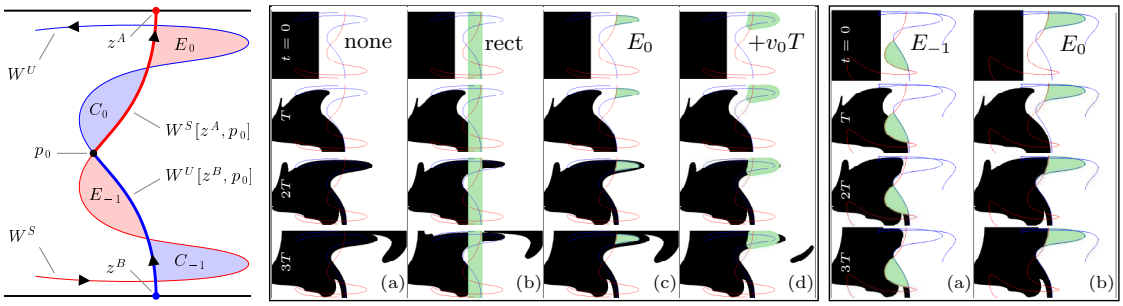

FIGURE 1. Left: Turnstile describing fluid transport across the bay mouth. Middle: Algae invades from the left. Illustration of control and three treatment protocols. Right: Algae treatment based on burnstile lobes is effective and efficient.

In a fashion analogous to the advective case, we combine segments of stable and unstable BIM to form the *burnstile*. This structure correctly describes the mechanism by which front propagation to the right is facilitated by the flow. Specifically, it provides efficient treatment protocols that entirely prevent the algae invasion.

This simple theory raises as many questions as it answers. We conclude with a few of these questions.

In Fig. 1(right), both the modified E_{-1} and E_0 lobes were used to prevent invasion. However, these lobes have different areas (this is not an area preserving system). Depending on system parameters, one or the other lobe may be larger. What more can be said about this lobe sequence? Is there just one locally smallest lobe? To what questions are the other lobes the answer? Does allowing for continuous time treatment offer more efficiency?

A burnstile (or turnstile) structure requires the existence of a primary intersection point (pip). What are the physical consequences of losing a pip? In particular, what is the relation between pip-free systems and "ballistic" front progress? Can the theory be amended to smoothly accommodate this loss?

A number of potential extensions suggest themselves: non-isotropic, non-homogenous front speed; curvature-dependent front speed; and maybe of most significance, fuzzy fronts, or simply diffusion in flows.

Acknowledgements. The present work was supported by the US National Science Foundation under grants PHY-0748828 and CMMI-1201236.

REFERENCES

[1] S. Wiggins, *Chaotic Transport in Dynamical Systems*, Springer, 1992.
[2] J.R. Mahoney and K.A. Mitchell, *A turnstile mechanism for fronts propagating in fluid flows*, Chaos **23** (2013), 043106.
[3] J. Mahoney, D. Bargteil, M. Kingsbury, K. Mitchell and T. Solomon, *Invariant barriers to reactive front propagation in fluid flows*, EPL **98** (2012), 44005.
[4] K.A. Mitchell and J. Mahoney, *Invariant manifolds and the geometry of front propagation in fluid flows*, Chaos **22** (2012), 037104.

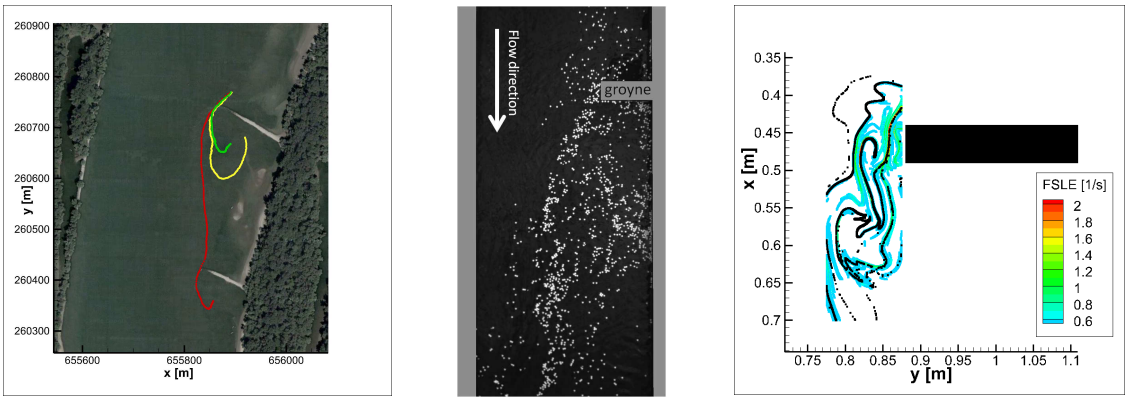

FIGURE 1. Left: Trajectories of three surface buoys in River Danube in the vicinity of a groyne field. Middle: Laboratory setup with a single groyne and the floating particles used for the PTV- measurements. Right: FSLE ridges (colored) and the largest flushing times (black) at $t = 0$s. The groyne is marked as a black rectangle.

[5] D. Bargteil and T. Solomon, *Barriers to front propagation in ordered and disordered vortex flows*, Chaos **22** (2012), 037103.

Metamorphosis of stable manifolds in unsteady aperiodic river flows

MÁRTON ZSUGYEL
(joint work with Tamás Tél and János Józsa)

Field measurements around a sequence of groynes were carried out [1] in River Danube in order to characterize mixing. GPS-equipped floating buoys were released close to each other, see Fig. 1(left), and the buoy-pair distance evolutions were analyzed. The available low number of buoys indicated chaotic spreading in the vicinity of the groynes. For a detailed characterization of the mechanisms we carried out appropriate (PTV-based) laboratory measurements, see Fig. 1(middle), too. This provided a surface velocity field in which millions of numerical particle trajectories were simulated and chaotic indicators were calculated.

The stable manifold of a (moving) saddle point is visualized at a given time as the set of initial positions characterized with the largest flushing time (black line in Fig. 1(right)) around a groyne head, i.e. the time elapsing until the particle flows out of the observation area. We can see that the ridges (reddish colors in Fig. 1(right)) of the Finite-Size Lyapunov exponent (FSLE) field approximately coincide with the largest flushing times. In a detailed study we demonstrated how particles starting from the black line of Fig. 1(right) at $t = 0$s converge along a time-dependent stable manifold of an ever changing shape to a chaotic saddle by time $t = 18$s and finally separate again along an unstable manifold by time $t = 36$s [2].

Similar stable manifold metamorphoses are expected to occur in any fluvial environment with strong shear zones.

References

[1] M. Zsugyel, K.G. Szabó, Zs.M. Kiss, J. Józsa, G. Ciraolo, C. Nasello, E. Napoli and T. T'el, *Detecting chaotic nature of advection in complex river flows*, Per. Pol. Civil Eng. **56** (2012), 97–106.

[2] M. Zsugyel, T. Tél and J. Józsa, *Numerical investigation of chaotic advection past a groyne based on laboratory flow experiments*, Ad. Water Res. submitted.

Finite-Size Lyapunov Exponents and Lagrangian Coherent Structures

Daniel Karrasch

(joint work with George Haller)

The Finite-Size Lyapunov Exponent (FSLE) is a popular Lagrangian diagnostic of trajectory separation in finite-time dynamical systems. The FSLE infers a local separation exponent for each initial condition x_0 over a different time interval of length $\tau(x_0;\delta_0,r)$, i.e. the *separation time*. Here, $\delta_0>0$ is the initial distance of neighboring particles and $r>1$ is a *separation factor* of interest; see [1] for more details and references. Another popular Lagrangian diagnostic is the Finite-Time Lyapunov Exponent (FTLE), for which integration time is fixed and the separation of infinitesimal neighbors is measured.

The FSLE has been used in the detection of specific coherent flow features. In particular, ridges of the FSLE field have been proposed as indicators of hyperbolic Lagrangian Coherent Structures (LCS), which are most repelling or most attracting material surfaces over a given time interval $[t_0,t]$. This idea is based on a heuristic analogy with the FTLE field and an observed visual similarity of the FSLE and FTLE fields, cf. [2] and Peikert's abstract in this report.

In [1], we discuss in detail some marked differences between the FSLE and FTLE that contradict the broadly presumed equivalence of these two scalar fields. The differences stem from irregularities of the FSLE field, which include local ill-posedness, spurious ridges, insensitivity to changes in the dynamics past the separation time, and intrinsic jump-discontinuities.

We also establish mathematical conditions under which select FSLE ridges do signal the presence of nearby FTLE ridges, which in turn mark hyperbolic LCS under further conditions. To that end, we introduce a new separation metric, the Infinitesimal-Size Lyapunov Exponent (ISLE), as the $\delta_0\to 0$ limit of the FSLE. We also show examples in which FSLE ridges fail to satisfy our conditions, and indeed do not correspond to nearby FTLE ridges.

References

[1] D. Karrasch and G. Haller, *Do Finite-Size Lyapunov Exponents Detect Coherent Structures?*, Chaos **23** (2013), 043126.

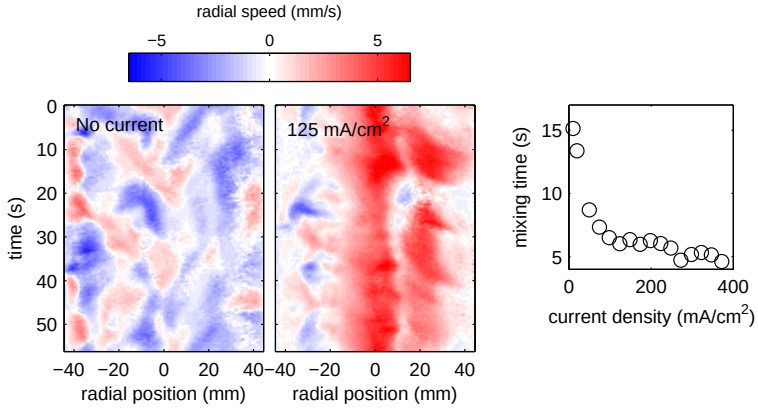

FIGURE 1. Ultrasound measurements of flow in a liquid metal electrode, without current and with current density 125 mA/cm^2. The presence of current speeds and organizes the thermal convection. Additional measurements at other current densities show that mixing time decreases as current density increases, with a sharp onset near 50 mA/cm^2. Faster mixing improves battery rate capability.

[2] R. Peikert, A. Pobitzer, F. Sadlo and B. Schindler, *A Comparison of Finite-Time and Finite-Size Lyapunov Exponents*, In *Topological Methods in Data Analysis and Visualization III*, Springer, 2014.

Mixing and coherent structures in a liquid metal electrode

DOUGLAS KELLEY
(joint work with Donald R. Sadoway)

Coherent structures open the way for analysis and control of complex systems. One system of interest is the liquid metal battery [1, 2], a new and economic technology for grid-scale storage of electrical energy. Adding storage capacity to Earth's electrical grids would dramatically reduce cost and improve reliability by accommodating short-term demand variations and enabling the broad deployment of wind and solar generation. Because these batteries are entirely liquid, mixing directly affects battery performance: their rate-limiting process is mass transport in the positive electrode, and flow is driven by both thermal and electromagnetic forces. We use ultrasound velocimetry to measure mixing in a liquid metal electrode and study its variation with electrical current density, as shown in Fig. 1. We find that the flow becomes more ordered and faster when current density exceeds a threshold value. Our observations are consistent with previous studies of magnetoconvection and imply that electrical current promotes mixing, which improves battery performance. Next we will build stochastic system models similar to those recently developed for convection [3].

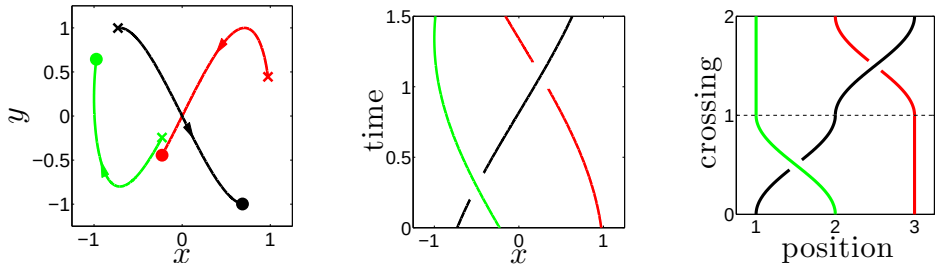

FIGURE 1. Left: Trajectories. Middle: Space-time projection. Right: Crossing map. Taken from [2].

REFERENCES

[1] D.J. Bradwell, H. Kim, A.H.C. Sirk and D.R. Sadoway. *Magnesium-antimony liquid metal battery for stationary energy storage*, J. Am. Chem. Soc. **134** (2012), 1895–1897.

[2] H. Kim, D.A. Boysen, J.M. Newhouse, B.L. Spatocco, B. Chung, P.J. Burke, D.J. Bradwell, K. Jiang, A.A. Tomaszowska, K. Wang, W. Wei, L.A. Ortiz, S.A. Barriga, S.M. Poizeau and D.R. Sadoway. *Liquid metal batteries: Past, present, and future*, Chem. Rev. **113** (2013), 2075–2099.

[3] E. Brown and G. Ahlers. *Large-scale circulation model for turbulent Rayleigh-Bénard convection*, Phys. Rev. Lett. **98** (2007), 134501.

Investigations of the braid theory approach for identifying coherent structures

MARGAUX FILIPPI

(joint work with Thomas Peacock, Jean-Luc Thiffeault, Michael Allshouse, Marko Budišić)

Knowledge of the ocean surface dynamics is crucial to many areas of oceanography, ranging from marine ecology to heat transport and climate. To better understand surface mixing, we survey methods to detect Lagrangian Coherent Structures (LCS), which are barriers to transport between distinct dynamical regions in the flow. Whereas most techniques rely on an extensive knowledge of the flow field, we seek methods to detect LCS from sparse data sets, such as floats trajectories. Based on the work of Jean-Luc Thiffeault [1] and Michael Allshouse [2], we investigate transport barriers from drifter trajectories with braid theory.

Consider sparse floaters drifting at sea, and map their trajectories onto a plane, as illustrated in Fig. 1(left). Now project them onto a space-time plane, representing each trajectory by a strand evolving with time (see Fig. 1(middle)). Because of the physical nature of the drifters, the trajectories do not intersect. However, the strands can entangle, or *cross*. We then construct a *braid*: a geometric object consisting of non-intersecting strands evolving with time, with sequenced crossings. Fig. 1(right) shows the braid representation of the initial trajectories.

Next, we assign indices and directions to the crossings: define σ_i (σ_i^{-1}) as the clockwise (counter-clockwise) crossing between the i^{th} and $(i+1)^{th}$ strands, when viewed from the top. Then, the braid diagram in Fig. 1(rigth) is translated to

$\sigma_1\sigma_2^{-1}$. We thus build blocks of crossings written as sequences of crossings: the initial geometric data is thereby expressed algebraically. Now, consider three particles and a material line, or loop, initially wrapped tightly around two of the particles. By interchanging the particles according to the braid crossing sequence above, the line is stretched. With iterations of the action of the braid, the length of the line grows exponentially. From the braid crossing sequence, we infer the material line growth rate, which enables us to determine the degree of entanglement of the initial trajectories. Finally, coherent structures are defined by particle trajectories that travel together and do not entangle. Transport barriers can be identified using the growth of line around trajectories and looking at regions with slow rates. Allshouse and Thiffeault refined the method: the *pair-loop* algorithm they developed [2] looks at pairs of trajectories. For each pair, the crossing sequence is calculated and applied to the loop enclosing this pair. This method then finds the particles entangled by each loop and determines which particles lie within invariant regions.

To study the chaotic advection of fluid particles on a plane, we use Hackborn's [3] rotor-oscillator, which consists of a rotating cylinder (rod) and its longitudinal oscillation. This system has also been used to study flow separation by Weldon et al [4]. The velocity field is defined by a stream function as given by Hackborn:

$$\psi(x,y) = \frac{1}{2}\log[f(x,y)] + \int_0^\infty g(x,k)\cos(ky)\,\mathrm{d}k, \tag{1}$$

with the y-axis parallel to the axis of oscillation, c the initial rod position, and:

$$f(x,y) = \frac{1 - 2\mathrm{e}^{\frac{\pi y}{2}}\cos[\frac{\pi(x-c)}{2}] + \mathrm{e}^{\pi y}}{1 + 2\mathrm{e}^{\frac{\pi y}{2}}\cos[\frac{\pi(x+c)}{2}] + \mathrm{e}^{\pi y}},$$

$$g(x,k) = \frac{2[\tanh k\cosh kx - x\sinh kx]\cosh kc}{\sinh 2k + 2k} + \\ + \frac{2[\coth k\sinh kx - x\cosh kx]\sinh kc}{\sinh 2k - 2k}.$$

Fig. 2 shows the calculated field for a non-dimensional rotor-oscillator flow. Trajectories are then analyzed in `braidlab`, a matlab module developed by Thiffeault.

References

[1] J.-L. Thiffeault, *Braids of entangled particle trajectories*, Chaos **20** (2010), 017516.

[2] M.R. Allshouse and J.-L. Thiffeault, *Detecting coherent structures using braids*, Physica D **241** (2012), 95–105.

[3] W.W. Hackborn, M.E. Ulucakli and T. Yuster, *A theoretical and experimental study of hyperbolic and degenerate mixing regions in a chaotic Stokes flow*, J. Fluid Mech. **346** (1997), 23–48.

[4] M. Weldon, T. Peacock, G.B. Jacobs, M. Helu and G. Haller, *Experimental and numerical investigation of the kinematic theory of unsteady separation*, J. Fluid Mech. **611** (2008), 1–11.

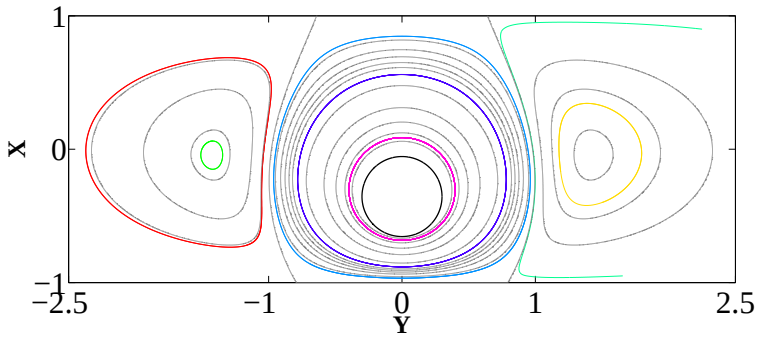

FIGURE 2. Streamlines and trajectories for ψ as in Eq. (1), and initial rod position.

The asymptotic dynamics of inertial particles with memory

MOHAMMAD FARAZMAND
(joint work with Gabriel P. Langlois, George Haller)

The motion of finite-size (or inertial) particles moving in an ambient fluid flow is of interest in many engineering and environmental applications. The inertial particle dynamics is modeled by the Maxey–Riley (MR) equation [1]

$$\dot{y} = u(y,t) + w(t),$$

$$\dot{w} + \kappa\mu^{1/2}\frac{\mathrm{d}}{\mathrm{d}t}\int_{t_0}^{t}\frac{w(s)}{\sqrt{t-s}}\,\mathrm{d}s + \mu w = -\nabla u(y,t)w + \mathrm{R}\left[\frac{\mathrm{D}u}{\mathrm{D}t}(y,t) - \mathrm{g}\right], \tag{1}$$

which describes the motion of a small spherical particle. Here, $y\colon \mathbb{R}^+ \to \mathcal{D}$ represents the particle position and $w\colon \mathbb{R}^+ \to \mathbb{R}^n$ is the instantaneous deviation of the particle velocity from the fluid velocity u. The constants $\mu \gg 1$, R and κ are dimensionless parameters and g is dimensionless gravitational acceleration. The total derivatives $\frac{\mathrm{D}}{\mathrm{D}t}$ and $\frac{\mathrm{d}}{\mathrm{d}t}$ refer to derivatives along fluid and particle trajectories, respectively. Therefore, $\frac{\mathrm{D}u}{\mathrm{D}t}$ is the acceleration of the fluid.

To simplify the equation, the fractional-order derivative $\kappa\mu^{1/2}\frac{\mathrm{d}}{\mathrm{d}t}\int_{t_0}^{t}\frac{w(s)}{\sqrt{t-s}}\,\mathrm{d}s$ (also referred to as the *memory term*) has been routinely neglected in the studies of inertial particle dynamics. Recent experimental and numerical studies (see [2] and references therein), however, indicate some important qualitative changes in the behavior of the solutions of MR in the presence of the memory term.

Here we present an analytic study of the impact of the fractional-order derivative on the solutions of the MR equation. In particular, we show that the fractional-order derivative changes some fundamental properties of the solutions including smoothness [3], asymptotic behavior and the convergence rate to this asymptotic state.

Rescaling time by introducing $\tau = t/\epsilon$ where $\epsilon = 1/\mu \ll 1$, we find an equivalent integral equation for (1). Applying a Gronwall-type inequality [4] to this integral equation we get the following result.

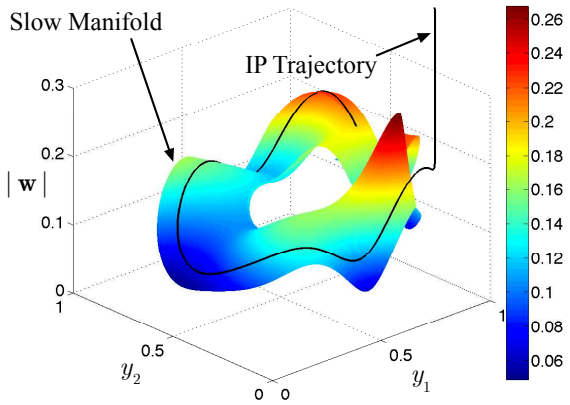

FIGURE 1. Convergence of an inertial particle (IP) to the slow manifold. The magnitude of the relative velocity $|w|$ is shown along a trajectory $y = (y_1, y_2)$ of the MR equation (1). The ambient fluid flow is a periodically forced double gyre [5]. The slow manifold is visualized as a surface in the space $(y_1, y_2, |w|)$.

Theorem 1. *Assume* $\|\nabla u\|_\infty < M_1$, $2\|\frac{\mathrm{D}u}{\mathrm{D}t} - \mathrm{g}\|_\infty < M_2$ *and* $\epsilon < \frac{1}{M_1}$. *Then we have*

(i) $|w(\tau)| \leq \frac{|w_0|+\epsilon M_2}{1-\epsilon M_1}$, $\forall \tau \geq 0$,
(ii) $|w(\tau)| \leq \epsilon M_2/(1-\epsilon M_1)$, *for* τ *large enough,*

where $w_0 = w(t_0)$ *is the initial relative velocity.*

A corollary of the above theorem is that the set $\{(y, w, t) : |w| \leq \epsilon M_2/(1-\epsilon M_1)\}$ is an asymptotically attracting invariant set for the MR equation (1). Moreover, the rate of convergence to this set can be shown to be algebraic: $t^{-3/2}$. Numerical simulations suggest the existence of a globally attracting slow manifold in this set (see Fig. 1).

REFERENCES

[1] M.R. Maxey and J.J. Riley, *Equation of motion for a small rigid sphere in a nonuniform flow*, Phys. Fluids **26** (1983), 883–889.
[2] A. Daitche and T. Tél, *Memory Effects are Relevant for Chaotic Advection of Inertial Particles*, Phys. Rev. Lett. **107** (2011), 244501.
[3] M. Farazmand and G. Haller, *The Maxey-Riley Equation: Existence, Uniqueness and Regularity of Solutions*, submitted preprint, available from `arxiv.org/abs/1310.2450`.
[4] S.C. Chu and F.T. Metcalf, *On Gronwall's inequality*, Proc. of American Math. Society. **18** (1967), 439–440.
[5] S.C. Shadden, F. Lekien, J. E. Marsden, *Definition and properties of Lagrangian coherent structures from finite-time Lyapunov exponents in two-dimensional aperiodic flows*, Physica D **212** (2005), 271–304.

Lagrangian Coherent Structures from Video Streams of Jupiter

Alireza Hadjighasem
(joint work with George Haller)

1. Introduction

Jupiter's fast rotation - one rotation over 10 hours - creates strong jet streams, smearing its clouds into linear bands of dark and light zonal belts that circle the planet on lines of almost constant latitude. Such a high degree of axisymmetry is absent in our own atmosphere. Moreover, Jupiter has the largest and longest-living known atmospheric vortex, the Great Red Spot (GRS). Such vortices abound in nature, but GRS's size, long-term persistence, and temporal longitudinal oscillations make it unique.

Here, we uncover, for the first time, unsteady material structures that form the cores of zonal jets and the boundary of the GRS in Jupiter's atmosphere. We perform our analysis on a velocity field extracted from a video footage acquired by the NASA Cassini spacecraft.

2. Background: Lagrangian coherent structures

Consider a two-dimensional unsteady velocity field

$$\dot{x} = v(x,t), \quad x \in U \subset \mathbb{R}^2, \quad t \in [t_0, t], \tag{1}$$

which defines a two-dimensional flow over the finite time interval $[t_0, t]$ in the spatial domain U. The flow map $F_{t_0}^t(x_0) : x_0 \mapsto x_t$ of (1) then maps the initial condition x_0 at time t_0 to its evolved position x_t at time t. The Cauchy–Green (CG) strain tensor associated with (1) is defined as

$$C_{t_0}^t(x_0) = {DF_{t_0}^t}^\top DF_{t_0}^t,$$

where $DF_{t_0}^t$ denotes the gradient of the flow map, and the symbol $\top$ indicates matrix transposition. The CG strain tensor is symmetric and positive definite, thus has two positive eigenvalues $0 < \lambda_1 \leq \lambda_2$ and an orthonormal eigenbasis $\{\xi_1, \xi_2\}$, defined as

$$C_{t_0}^t(x_0)\xi_i(x_0) = \lambda_i(x_0)\xi_i(x_0), \qquad |\xi_i(x_0)| = 1, \qquad i \in \{1,2\}.$$

We shall suppress the dependence of CG invariants on t_0 and t for notational simplicity.

A general material line (composed of an evolving curve of initial conditions) experiences both shear and strain in its deformation. As argued in [1, 2], the averaged straining and shearing experienced within a strip of ϵ-close material lines will generally differ by an $\mathcal{O}(\epsilon)$ amount over a finite time interval due to the continuity of the finite-time flow map.

We seek a Lagrangian Coherent Structure (LCS) as an exceptional material line around which $\mathcal{O}(\epsilon)$ material belts show no $\mathcal{O}(\epsilon)$ variation in the length-averaged Lagrangian shear or strain over the time interval $[t_0, t]$. This implies that an LCS is a stationary curve for the averaged Lagrangian shear or strain functionals.

2.1. **Shearless LCS: stationary curves of averaged shear.** Specifically, a shearless LCS is a material line whose averaged shear shows no leading order variation with respect to the normal distance from the LCS. Farazmand et al. [1] show that such curves are null-geodesics of a Lorentzian metric. The most robust class of these null-geodesics turns out to be composed of smooth chains of tensorlines (trajectories of the eigenvector fields of CG) that connect singularities of the CG field. Out of all such possible chains, one builds parabolic LCS (generalized jet cores) by identifying tensorlines closest to being neutrally stable (cf. [1] for details).

2.2. **Strainless LCS: stationary curves of averaged strain.** Similarly, a strainless LCS is a material line whose averaged strain shows no leading order variation with respect to the normal distance from the LCS. As shown by Haller and Beron-Vera [2], such stationary curves of the tangential stretching functional coincide with the null-geodesics of another Lorentzian metric that are tangent to one of the vector fields

$$\eta_\lambda^\pm(x_0) = \sqrt{\frac{\lambda_2(x_0)-\lambda^2}{\lambda_2(x_0)-\lambda_1(x_0)}}\xi_1(x_0) \pm \sqrt{\frac{\lambda^2-\lambda_1(x_0)}{\lambda_2(x_0)-\lambda_1(x_0)}}\xi_2(x_0), \tag{2}$$

We refer to closed orbits (limit cycles) of the vector fields (2) as elliptic LCS. The outermost orbit of such a family of limit cycles serves as a coherent Lagrangian vortex boundary. It is infinitesimally uniformly stretching, i.e., any of its subsets stretches exactly by a factor of λ over the time interval $[t_0, t]$. Limit cycles of $\eta_\lambda^\pm(x_0)$ only tend to exist for $\lambda \approx 1$, guaranteeing a high degree of material coherence for the Lagrangian vortex boundary.

3. Results

We used the ACCIV algorithm of Asay-Davis et al. [3] to extract a time-resolved atmospheric velocity field from video footage taken by the NASA Cassini Orbiter. The ACCIV algorithm yields a high density of wind velocity vectors, which is advantageous over the limited number of vectors traditionally obtained from manual cloud tracking.

Observational records of Jupiter go back to the late 19th century, indicating that Jupiter's atmosphere is highly stable in the latitudinal direction. Therefore, the average zonal velocity profile as a function of latitudinal degree is an important benchmark for examining the quality of the reconstructed velocity field.

In Fig. 1A, we compare our temporally averaged zonal velocity profile obtained form ACCIV algorithm with the profile reported by Limaye [4]. Limaye's profile is based on Voyager I and Voyager II images, covering 144 Jovian days. Our velocity profile is based on video footage captured by Cassini Orbiter during its flyby in route to Saturn in 2000, just covering 24 Jovian days. Despite these differences in the data, the two profiles show sufficiently close agreement.

Using the extracted time-resolved velocity, we applied the geodesic theory of LCS reviewed in Section 2 to the detection of a coherent Lagrangian boundary for the GRS, and of the cores of eastward- and westward-moving zonal jets (Fig. 1B). Advected images (not shown here) of the extracted LCS confirm their sustained

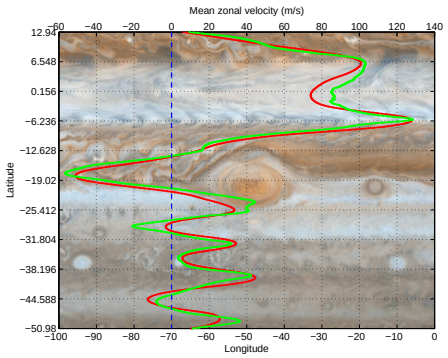

(A) Zonal velocity profile of Jupiter's atmosphere. The red line is our velocity profile which is obtained from Cassini images, and the green profile is the velocity profile reported by S.S. Limaye [4].

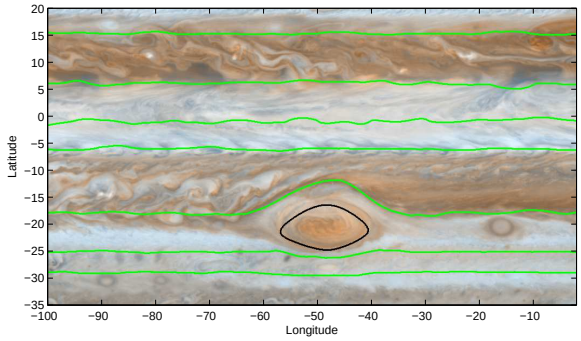

(B) Shearless LCS (green) as zonal jet cores, and an elliptic LCS (black) as the Lagrangian boundary of the Great Red Spot. (Background image credit: NASA/JPL-Caltech)

FIGURE 1

coherence and organizing role in cloud transport and mixing. We will report further details and results elsewhere.

REFERENCES

[1] M. Farazmand, D. Blazevski and G. Haller, *Shearless transport barriers in unsteady two-dimensional flows and maps*, Physica D, submitted.

[2] G. Haller and F.J. Beron-Vera, *Coherent Lagrangian vortices: the black holes of turbulence*, J. Fluid Mech. **731** (2013), R4.

[3] XS. Asay–Davis, P.S. Marcus, M.H. Wonga and I. de Patera, *Jupiter's shrinking Great Red Spot and steady Oval BA: Velocity measurements with the 'Advection Corrected Correlation Image Velocimetry' automated cloud-tracking method*, Icarus **203** (2009), 164–188.

[4] S.S. Limaye, *Jupiter - New estimates of the mean zonal flow at the cloud level*, Icarus **65** (1986), 335–352.

Distribution of particle displacements in biomixing

JEAN-LUC THIFFEAULT

The experiments of Leptos *et al.* [1] show that the displacements of small particles affected by swimming microorganisms achieve a non-Gaussian distribution, which nevertheless scales diffusively. We use a simple model where the particles undergo repeated 'kicks' due to the swimmers to explain the shape of the distribution.

Leptos *et al.* study the microscopic algae *Chlamydomonas reinhardthii*. They measure experimentally the probability density function (PDF) of tracer displacements, $\rho_{X_t}(x)$. Thus, $\rho_{X_t}(x)\,\mathrm{d}x$ is the probability of observing a particle displacement $X_t \in [x, x+\mathrm{d}x]$ after waiting a time t. The range of t is chosen small enough that the swimmers are 'ballistic,' so their velocity is roughly constant.

At zero volume fraction ($\phi = 0$), the distribution $\rho_{X_t}(x)$ is Gaussian, due solely to molecular diffusivity. For higher number densities, exponential tails appear and the Gaussian core broadens. Leptos *et al.* fit their the distribution to the sum of a Gaussian and an exponential:

$$\rho_{X_t}(x) = \frac{1-f}{\sqrt{2\pi\delta_g^2}}\,\mathrm{e}^{-x^2/2\delta_g^2} + \frac{f}{2\delta_e}\,\mathrm{e}^{-|x|/\delta_e}.$$

They observe the scalings $\delta_g \sim A_g t^{1/2}$ and $\delta_e \sim A_e t^{1/2}$, where A_g and A_e depend on ϕ. They call this a *diffusive scaling*, since $x \sim t^{1/2}$. Their point is that this is surprising, since the distribution is not Gaussian.

Our goal is to derive the PDF of displacements $\rho_{X_t}(x)$ from a simple model. We use the model described by Thiffeault & Childress [2] and improved by Lin *et al.* [3], which in spite of its simplicity captures the important features observed in experiments.

We assume there are N swimmers in a volume V, so the number density of swimmers is $n = N/V$. Initially, each swimmer travels at a speed U in a uniform random direction. They keep moving along a straight path for a time τ, so that each traces out a segment of length $\lambda = U\tau$. After this a new direction is chosen randomly and uniformly, and the process repeats—each swimmer again moves along a straight path of length λ. Though far from realistic, this model captures many essential features of the system, as found in [2, 3].

We wish to follow the displacement of an arbitrary 'target fluid particle.' The swimmers are all simultaneously affecting this fluid particle, but in practice only the closest swimmers significantly displace it. It is thus convenient to introduce an imaginary 'interaction sphere' of radius R centered on the target fluid particle, and count the number M_t of 'interactions,' that is the number of times a swimmer enters this sphere. (Our treatment applies to two-dimensional systems simply by changing 'sphere' to 'disk' and 'volume' to 'area.') Fig. 1A illustrates the situation.

When Nt/τ is large and R is not too large, the distribution of M_t is well approximated by a Poisson distribution:

$$\mathbb{P}\{M_t = M\} \simeq \frac{1}{M!}\langle M_t\rangle^M \mathrm{e}^{-\langle M_t\rangle}, \tag{1}$$

where the mean is given by the volume swept by the interaction sphere in time t:

$$\langle M_t\rangle \simeq n\pi R^2 \lambda\,(t/\tau). \tag{2}$$

Let us now consider these probabilities within the context of the Leptos *et al.* [1] experiments. The velocity of the swimmers is peaked at around $U \sim 100\,\mu$m/s. Their volume fraction is less than 2.2%. Assuming spherical organisms of radius $5\,\mu$m, this gives a number density $n \simeq 4.2\times10^{-5}\,\mu\mathrm{m}^{-3}$. The maximum observation time is about $t \sim 0.3\,$s, so that a typical swimmer moves by a distance $\lambda \sim 30\,\mu$m. From (2), we find

$$\langle M_t\rangle \simeq .004 \times (R/1\,\mu\mathrm{m})^2.$$

Hence, for $R = 20\,\mu$m (an interaction disk with a radius four times the swimmer's), we have $\langle M_t\rangle \simeq 1.58$. This is at the highest densities used in the experiments.

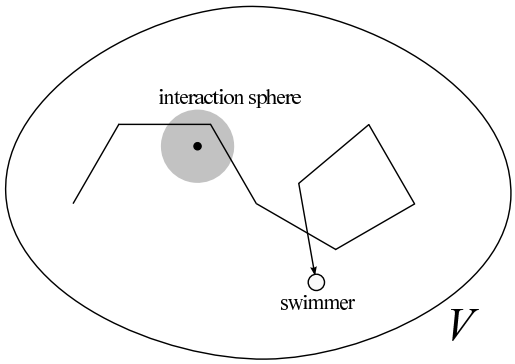

(A) A swimmer moving inside a volume V along a series of straight paths, each of length λ and in a uniform random direction.

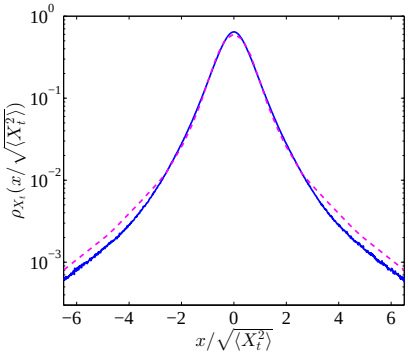

(B) The PDF of particle displacements obtained from Eq. (3) by sampling from single-swimmer displacements. The data from Leptos *et al.* [1] is the dashed line.

FIGURE 1

We conclude that a typical fluid particle is only strongly affected by about one swimmer. The only displacements that a particle feels 'often' are the very small ones due to all the faraway swimmers. We thus expect the displacement PDF to have a central Gaussian core (since the central limit theorem will apply for the small displacements), but strongly non-Gaussian tails. This is what is observed, and we will spend the remainder of the talk making this more precise.

Now that we have examined how often swimmers interact with a sphere of radius R centered around a target particle, we will look at how the particle gets displaced. Following Lin *et al.* [3], we start from a distribution of displacements $\Delta_\lambda \geq 0$ induced by a single swimmer. Each time a swimmer enters the interaction sphere we have an 'encounter,' which causes a displacement of the target particle in a random direction ψ_k; thus, after M encounters, the displacement in some fixed direction is

$$X_M = \sum_{k=1}^{M} \Delta_\lambda \cos\psi_k,$$

where each encounter has random i.i.d. values of the displacement Δ_λ.

The probability density of X_M is related to that of X_t, the displacement after a time t, by

$$\rho_{X_t}(x) = \sum_{M=0}^{\infty} \rho_{X_M}(x)\, \mathbb{P}\{M_t = M\}, \tag{3}$$

where $\mathbb{P}\{M_t = M\}$ is given by Eq. (1). Fig. 1B shows the PDF $\rho_{X_t}(x)$, normalized to unit standard deviation. The PDF was obtained by sampling from the single-swimmer displacements Δ_λ for a squirmer-type swimmer [3]. The fit to the data is good, though the tails are a bit depressed. This may be due to the use of a swimmer

model that entrains particles slightly less far than the actual organism. Eckhardt & Zammert [4] have obtained better fit by invoking an anomalous diffusion model. In a future publication we will investigate whether our model can account for more details of the Leptos *et al.* experiment.

References

[1] K.C. Leptos, J.S. Guasto, J.P. Gollub, A.I. Pesci and R.E. Goldstein, *Dynamics of enhanced tracer diffusion in suspensions of swimming eukaryotic microorganisms*, Phys. Rev. Lett. **103** (2009), 198103.

[2] J.-L. Thiffeault and S. Childress, *Stirring by swimming bodies*, Phys. Lett. A **374** (2010), 3487.

[3] Z. Lin, J.-L. Thiffeault and S. Childress, *Stirring by squirmers*, J. Fluid Mech. **669** (2011), 167.

[4] B. Eckhardt and S. Zammert, *Non-normal tracer diffusion from stirring by swimming microorganisms* Europ. Phys. J. E **35** (2012), 96–97.

Transfer operator approaches to identifying and tracking coherent structures and quantifying mixing and transport

Gary Froyland

The study of transport and mixing processes in dynamical systems is particularly important for the analysis of mathematical models of physical systems. In the autonomous setting, the use of transfer operators (PerronFrobenius operators) to identify invariant and almost-invariant sets, which are barriers to transport and mitigate mixing, has been particularly successful, with applications to molecular dynamics, astrodynamics, physical oceanography, and fluid dynamics. In the nonautonomous (time-dependent) setting, coherent sets [1, 2], a time-parameterised family of minimally dispersive sets, are a natural extension of almost-invariant sets. The present work introduces a new analytic transfer operator construction [3] that enables the calculation of finite-time coherent sets (sets are that minimally dispersive over a finite time interval). This new construction also elucidates the role of diffusion in the calculation and we show how properties, such as the spectral gap of the constructed operator and the regularity of singular vectors, scale with noise amplitude. The construction can also be applied to general Markov processes on continuous state space. In the presence of hyperbolic dynamics we demonstrate numerically that under increasing flow duration, the boundaries of coherent sets increasingly align with fundamental stable and unstable manifolds [4].

References

[1] G. Froyland, S. Lloyd and A. Quas, *Coherent structures and isolated spectrum for Perron-Frobenius cocycles*, Ergodic Theory Dynam. Systems **30** (2010), 729–756.

[2] G. Froyland, S. Lloyd and N. Santitissadeekorn, *Coherent sets for nonautonomous dynamical systems*, Physica D **239** (2010), 1527–1541.

[3] G. Froyland, *An analytic framework for identifying finite-time coherent sets in time-dependent dynamical systems*, Physica D **250** (2013), 1–19.

[4] G. Froyland and K. Padberg-Gehle, *Almost-invariant and finite-time coherent sets: directionality, duration, and diffusion*, In *Ergodic Theory, Open Dynamics, and Coherent Structures*, Springer, 2014.

Self-consistency requirements for Lagrangian Coherent Structures

George Haller

1. Introduction

Lagrangian Coherent Structures (LCS) were originally defined in [2] as locally most attracting, repelling or shearing material surfaces. Such surfaces are expected to shape trajectory patterns in finite-time, aperiodic dynamical system. The LCS acronym has, however, also become a generally used term to describe visual patterns obtained from applications of various flow diagnostics.

Despite this trend, a diagnostic tool should satisfy a minimal set of mathematical self-consistency requirements before its output features can be called LCS. This is not unlike insisting on a minimal set of requirements that a heuristic numerical solver should satisfy before we refer to its output as a solution of a differential equation.

Here, we propose a set of self-consistency requirements for LCS detection, with a more detailed account appearing in [3].

2. Objectivity

A fundamental principle of mechanics is that material response should be independent of the observer [1]. This principle of objectivity prompts us to add Coriolis and centrifugal forces to Newton's equations in a rotating frame, so that the resulting material response by a particle is just the same as in an inertial frame.

LCS are all about describing coherence in material response. Any LCS definition or detection method should therefore be invariant under Euclidean coordinate-changes of the form

$$y = Q(t)x + p(t),$$

with $Q(t)$ denoting a time-dependent proper orthogonal tensor, and $p(t)$ denoting a time-dependent translation [4].

3. Finite-time nature

Fluid flows that call for LCS analysis typically evolve aperiodically in time, and the structures of interest in them have a finite life span. Over such finite times, classic asymptotic concepts, such as stability, stable and unstable manifolds, or chaotic advection become mathematically undefined.

An LCS detection principle should therefore rely on a correct finite-time adaption of these asymptotic concepts. This is often challenging to satisfy, as classic notions of stability and instability lose their distinguishing power over finite time intervals due to the continuity of the flow map.

4. Lagrangian invariance

The word Lagrangian in the LCS acronym implies that the structure identified as LCS evolves with the flow, forming an invariant manifold in the extended phase space.

Several diagnostic approaches assess flow coherence over sliding time windows $[t_0, t_0+T]$, with the initial time t_0 sweeping through the observational time period. This approach effectively analyzes a sequence of different finite-time dynamical systems, and the results from the analysis will not form an invariant manifold in the extended phase space for aperiodic flow.

5. Continuity

LCS approaches generally utilize diagnostic fields computed from the flow. These scalar field are meant to decide if any given trajectory belongs to an LCS or not. Consequently, an LCS diagnostic for smooth flows should at least be continuous, otherwise it will classify the same point differently under two different directions of approach.

LCS detection tools that apply the flow map to all initial conditions for the same length of time tend to be continuous. Diagnostic tools that apply the flow map to different initial condition over different time intervals may have intrinsic discontinuities.

References

[1] M.E. Gurtin, *An Introduction to Continuum Mechanics*, Academic Press, 1981.
[2] G. Haller and G. Yuan, *Lagrangian coherent structures and mixing in two-dimensional turbulence*, Physica D **147** (2000), 352-370.
[3] G. Haller, *Lagrangian Coherent Structures*, Ann. Rev. Fluid Mech., submitted.
[4] C. Truesdell and W. Noll, *The Non-Linear Field Theories of Mechanics*, Springer, 2004.

Differential descriptions for characteristic curves and their possible role in flow analysis

Tino Weinkauf
(joint work with Holger Theisel, Hans-Christian Hege)

The properties of a flow can be explained by considering the motion of particles. A particle moves with the flow on its *trajectory* or *path line*, which is a line consisting of all point locations visited by the particle over time. Real-world flow experiments often make use of other characteristic curves for visualization purposes: a *streak line* consists of a large number of particles, which have been injected into the flow one after another from the same location. A common way to achieve this effect in a flow lab is to constantly release smoke from a nozzle. It moves with the flow and thereby forms the streak line. A *time line* is another means of visualizing a flow. It is created by an instantaneous release of smoke from a slit: the initially straight line of smoke is transported by the flow and rolls up in vortices.

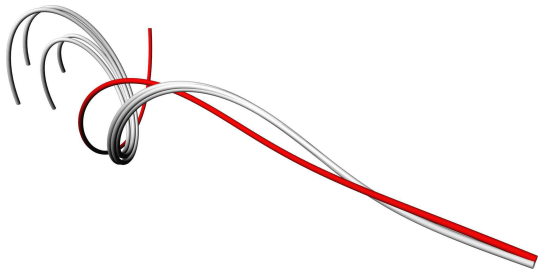

FIGURE 1. Vortex core line (red) in the center of swirling streak lines.

It is well-known that stream and path lines can be expressed using ordinary differential equations (ODE). This allows conclusions about important properties of these particle trajectories. For example, it is possible to determine their curvature without actually computing the trajectories themselves. Many important methods of computer-based flow analysis rely on the simple, yet powerful, representation of particle trajectories using ordinary differential equations. Other examples are steady-state topology and core lines around which particle trajectories exhibit a swirling motion.

The situation is different for streak and time lines. Existing descriptions are purely geometric, which does not allow conclusions about their inherent properties. We developed a general scheme to describe all four types of characteristic curves of flow fields - stream, path, streak, and time lines - as tangent curves of a derived vector field. Thus, all these lines can be obtained by a simple integration of an autonomous ODE system. Details can be found in our corresponding publications [1, 2].

With this differential description of characteristic curves, a large number of feature extraction and analysis tools becomes available for all types of characteristic curves, which were previously only available for stream and path lines. This is the case because the inherent properties of streak and time lines can now be expressed in a compact mathematical form.

Fig. 1 shows a core line in the center of swirling streak lines. This may lead to a new characterization of vortex structures. In [1], we describe how to find an attractor using this method, which cannot be found using many other methods including FTLE.

As a side effect, streak and time lines can often be computed significantly faster using the new approach. This gives rise to new possibilities in flow visualization. In [3], we describe an approach to create non-cluttered streak line visualizations, which strongly benefits from the faster computation scheme. Fig. 2 shows examples.

REFERENCES

[1] T. Weinkauf and H. Theisel, *Streak lines as tangent curves of a derived vector field*, IEEE TVCG (Proc. IEEE Visualization) **16** (2010), 1225–1234.

[2] T. Weinkauf, H.-C. Hege and H. Theisel, *Advected tangent curves: A general scheme for characteristic curves of flow fields*, Computer Graphics Forum **31** (2012), 825–834.

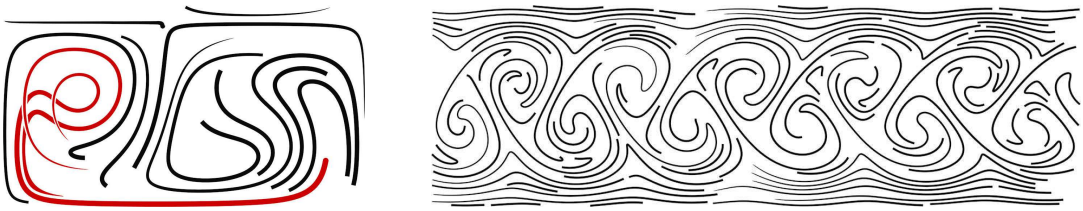

FIGURE 2. Uncluttered visualizations of streak lines in the double gyre (left) and in the flow behind a cylinder (right).

[3] T. Weinkauf, H. Theisel and O. Sorkine, *Cusps of Characteristic Curves and Intersection-Aware Visualization of Path and Streak Lines*, In *Topological Methods in Data Analysis and Visualization II*, Springer, 2012.

Spectral methods for computing Lagrangian coherent structures

CLARENCE W. ROWLEY
(joint work with Matthew O. Williams, Irina I. Rypina)

We present a method for determining finite-dimensional approximations of the Perron-Frobenius and Koopman operators directly from experimental data. The approach amounts to a spectral collocation method: one chooses any desired basis for the space of *observables* (functionals on the phase space), and test functions that are Dirac measures centered at the locations of the available data. The result is a finite dimensional approximation of the Koopman operator that can be directly used to approximate the Koopman eigenfunctions or slightly modified to reveal coherent structures such as almost invariant or coherent sets [2, 3]

Consider a discrete-time dynamical system evolving on a vector space, V, with dynamics $x \mapsto f(x)$. Let $\mathcal{F}$ be a vector space of functionals on V. The Koopman operator is a linear operator $\mathcal{K}\colon \mathcal{F} \to \mathcal{F}$ given by

$$\mathcal{K}\psi(x) = \psi(f(x)).$$

Now, suppose we have a (vector-valued) *observable*, a function $g\colon V \to \mathbb{R}^m$. If φ_j denote eigenfunctions of $\mathcal{K}$, then assuming we can expand

$$g(x) = \sum_{j=1}^{\infty} v_j \varphi_j(x),$$

these coefficients $v_j \in \mathbb{C}^m$ are called the *Koopman modes* associated with the observable g [4, 5].

Dynamic Mode Decomposition (DMD) was introduced in [7], and may be viewed as an algorithm for computing Koopman modes [5]. The version of the DMD algorithm used here is described in [8], and differs slightly from the original. Suppose one has two sets of data $\{x_1, \dots, x_n\}$, $\{y_1, \dots, y_n\}$ for $x_j, y_j \in V$, such that $y_j = f(x_j)$. Arrange the data into matrices

$$X = \begin{bmatrix} x_1 & x_2 & \cdots & x_n \end{bmatrix}, \qquad Y = \begin{bmatrix} y_1 & y_2 & \cdots & y_n \end{bmatrix},$$

and define the matrix

$$A = YX^+$$

where X^+ denotes the Moore-Penrose pseudoinverse. Then the DMD eigenvalues and DMD modes of the given dataset are the eigenvalues and eigenvectors of A. It is shown in [5, 8] that these approximate eigenvalues of the Koopman operator, and the corresponding Koopman modes v_j, for the observable $g(x) = x$. This is a useful algorithm for obtaining information about the Koopman operator directly from data; however, it does not give us an explicit approximation of the Koopman operator, or a method for computing Koopman *eigenfunctions*, φ_j.

We present a method we call Extended DMD, in which we approximate the Koopman operator using a weighted residual method. First, choose a basis $\{\psi_1, \ldots, \psi_N\}$ for a subspace $\mathcal{S}_N$ of $\mathcal{F}$, and expand any function $\varphi \in \mathcal{S}_N$ as

$$\varphi(x) = \sum_{j=1}^{N} a_j \psi_j(x),$$

where $a_j \in \mathbb{R}$. If $P_{\mathcal{S}_N}$ denotes a projection onto $\mathcal{S}_N$, we then expand

$$P_{\mathcal{S}_N} \mathcal{K} \varphi(x) = \sum_{j=1}^{N} b_j \psi_j(x),$$

where $b_j \in \mathbb{R}$. The approximate matrix representation of the Koopman operator is simply the matrix that maps $a = (a_1, \ldots, a_N)$ to $b = (b_1, \ldots, b_N)$. Defining a set of test functions $W_j \in \mathcal{F}^*$, for $j = 1, \ldots, M$, we have

$$b = \Psi_X^+ \Psi_Y a,$$

with

$$\Psi_X = \begin{bmatrix} \langle \psi_1, W_1 \rangle & \cdots & \langle \psi_N, W_1 \rangle \\ \vdots & & \vdots \\ \langle \psi_1, W_M \rangle & \cdots & \langle \psi_N, W_M \rangle \end{bmatrix},$$

$$\Psi_Y = \begin{bmatrix} \langle \psi_1 \circ f, W_1 \rangle & \cdots & \langle \psi_N \circ f, W_1 \rangle \\ \vdots & & \vdots \\ \langle \psi_1 \circ f, W_M \rangle & \cdots & \langle \psi_N \circ f, W_M \rangle \end{bmatrix}, \tag{1}$$

where $\langle \cdot, \cdot \rangle$ denotes the natural pairing. For arbitrary choices of W_j, these pairings or inner products may require a lot of data to compute. We pick

$$W_j(x) = \delta(x - x_j),$$

where δ is the Dirac measure and x_j is the j-th column of X. With this choice (which corresponds to a *collocation method*), Eq. (1) becomes

$$\Psi_X = \begin{bmatrix} \psi_1(x_1) & \cdots & \psi_N(x_1) \\ \vdots & & \vdots \\ \psi_1(x_M) & \cdots & \psi_N(x_M) \end{bmatrix}, \qquad \Psi_Y = \begin{bmatrix} \psi_1(y_1) & \cdots & \psi_N(y_1) \\ \vdots & & \vdots \\ \psi_1(y_M) & \cdots & \psi_N(y_M) \end{bmatrix}.$$

The approximate matrix representation of the Koopman operator is then

$$K = \Psi_X^+ \Psi_Y.$$

This choice of test functions, W_j, is a pragmatic one that allows the inner products to be computed directly from data. Another choice is a *Galerkin method*, in which $W_j = \psi_j$. Although the inner products in (1) are not computed explicitly, the Extended DMD method converges almost surely to a Galerkin method as $M \to \infty$ if a random sampling strategy is used. Therefore, the convergence of the finite dimensional approximation, K, to the Koopman operator, $\mathcal{K}$, is guaranteed as long as $\mathcal{S}_N \to \mathcal{F}$ as $N \to \infty$.

We illustrate the above method with a number of examples and using a variety of choices of basis functions. The method is equivalent to DMD if the basis functions are the components of the full state, $\psi_i(x) = \langle x, e_i \rangle$, where e_i denotes the i-th unit vector. However, we have also used Legendre polynomials, Fourier modes, indicator functions on rectangles (Ulam's method), radial basis functions, and simple spectral elements, which appear to be more versatile as they can represent larger subsets of $\mathcal{F}$. For a linear system, the Koopman eigenfunctions may be computed analytically, and we verify that the Extended DMD method recovers the exact eigenfunctions. We then use the method to compute isochrons of the van der Pol oscillator, and find almost-invariant sets and finite-time coherent sets in a double gyre example, using techniques in [3, 1, 2]. Finally, we use the method to compute coherent sets in the Philippine Sea, using trajectories from 200 simulated drifters, obtained from numerical simulations presented in [6].

References

[1] G. Froyland, *Statistically optimal almost-invariant sets*, Physica D **200** (2005), 205–219.

[2] G. Froyland, *An analytic framework for identifying finite-time coherent sets in time-dependent dynamical systems*, Physica D **250** (2013), 1–19.

[3] G. Froyland and M. Dellnitz, *Detecting and locating near-optimal almost-invariant sets and cycles*, SIAM J. Sci. Comput. **24** (2003), 1839–1863.

[4] I. Mezić, *Spectral properties of dynamical systems, model reduction and decompositions*, Nonlin. Dyn. **41** (2005), 309–325.

[5] C.W. Rowley, I. Mezić, S. Bagheri, P. Schlatter and D.S. Henningson, *Spectral analysis of nonlinear flows*, J. Fluid Mech. **641** (2009), 115–127.

[6] I.I. Rypina, S.E. Scott, L.J. Pratt, M.G. Brown and T. Tél, *Investigating the connection between complexity of isolated trajectories and Lagrangian coherent structures*, Nonl. Proc. Geophys. **18** (2011), 977–987.

[7] P.J. Schmid, *Dynamic mode decomposition of numerical and experimental data*, J. Fluid Mech. **656** (2010), 5–28.

[8] J.H. Tu, C.W. Rowley, D.M. Luchtenburg, S.L. Brunton and J.N. Kutz, *On dynamic mode decomposition: theory and applications*, preprint, available from `arxiv.org/abs/1312.0041`.

Network approaches to transport and mixing

Emilio Hernández-García
(joint work with Enrico Ser-Giacomi, Vincent Rossi and Cristóbal López)

Our understanding of transport and mixing in fluid flows has been greatly expanded in the last decades by focusing on Lagrangian approaches, that effectively consider trajectories of fluid particles as the orbits of dynamical systems.

One class of the techniques developed in this context, roughly labeled as *set-oriented* methods, considers the motion of regions of fluid in a probabilistic setting and assess properties such as invariance, coherence, or low leakage. The central tool is the *transfer matrix*, a discrete approximation to the Perron-Frobenius operator associated to the fluid flow, in which the fluid domain is discretized into small boxes. This approach has demonstrated its power to detect almost-invariant sets in abstract dynamical systems and in geophysical applications [1, 2], and has been generalized to track the motion of coherent moving sets also in oceanic flows [3].

Connectivity, internal and external coherence and mixing are important factors for the efficacy of Marine Protected Areas (MPAs) as biodiversity conservation tools. With this application in mind, we have applied set-oriented methods to the flow computed by the NEMO eddy resolving model of circulation in the Mediterranean Sea [4]. The aim was to extract oceanic regions which are well mixed internally but with weak mixing/exchange/connectivity with the surrounding waters. Whereas the standard methods to extract almost-invariant sets based on eigenvectors of the transfer matrix seem suited to this, we find two main limitations: First, the requirement of strong internal mixing is not explicitly taken into account. Second, the method in its simplest form seeks for partitions of the fluid domain into regions of similar size.

To overcome these limitations we realize that the representation of the flow in terms of a transfer matrix defines a *graph* or *network* in which nodes are the discrete boxes decomposing the fluid domain, and weighted and directed links are associated to each entry in the transfer matrix, giving an effective flow between them. We have access then to the great variety of powerful methods to partition a network into pieces according to different criteria, a task named *community detection* in the modern network theory literature [5]. Among the many algorithms available, we choose *Infomap* [6], because it overcomes the two above mentioned limitations, and because of its computational efficiency.

Fig. 1 shows an example of the partition obtained by the Infomap algorithm on the network defined by the transfer matrix in the Mediterranean for a 30-days flow. The colors denote values of the coherence ratio, which is the fraction of fluid remaining in the region after the considered period with respect the initial one. Note the diversity in sizes of the obtained regions. Adjustment of the integration times to time scales of biological relevance for marine larvae allows assessment of connectivity features of the MPAs already established in the Mediterranean, and provides new insightful information for the design of new ones [4].

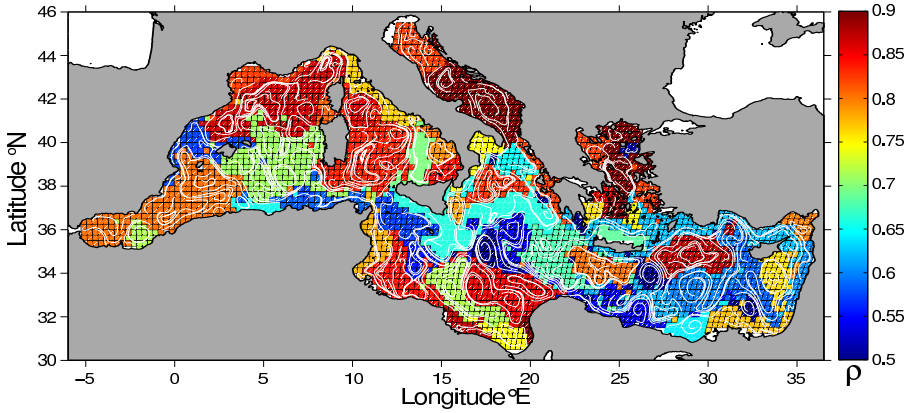

FIGURE 1. Partition of the Mediterranean into self-coherent regions by means of the Infomap algorithm applied to the network defined by a 30-days transfer matrix of surface Mediterranean flow. Colors give values of the coherence ratio ρ. White lines are mean streamlines.

REFERENCES

[1] G. Froyland and M. Dellnitz, *Detecting and locating near-optimal almost-invariant sets and cycles*, SIAM J. Sci. Comput. **24** (2003), 1839–1863.

[2] M. Dellnitz, G. Froyland, C. Horenkamp, K. Padberg-Gehle and A. Sen Gupta, *Seasonal variability of the subpolar gyres in the Southern Ocean: a numerical investigation based on transfer operators*, Nonlin. Processes Geophys. **16** (2009), 655–664.

[3] G. Froyland, C. Horenkamp, V. Rossi, N. Santitissadeekorn and A. Sen Gupta, *Three-dimensional characterization and tracking of an Agulhas ring*, Ocean Modelling **52-53** (2012), 69–75.

[4] V. Rossi, E. Ser-Giacomi, C. López and E. Hernández-García, *Hydrodynamic provinces and oceanic connectivity from a transport network help designing marine reserves*, to appear in Geophysical Research Letters, doi:10.1002/2014GL059540.

[5] S. Fortunato, *Community detection in graphs*, Physics Reports **486** (2010), 75–174.

[6] M. Rosvall, C. Berstrom, *Maps of random walks on complex networks reveal community structure*, Proceedings of the National Academy of Sciences **105** (2008), 1118–1123.

Stirring by microorganisms

BRUNO ECKHARDT
(joint work with Stefan Zammert)

The collisions between the molecules in a liquid and pollen grains causes the irregular motion of the grains that is known as Brownian motion. Since the kicks are uncorrelated, the dispersal of the grains follows the usual dispersal law $\langle x^2 \rangle \propto t$ and the probability density function (pdf) of the positions is Gaussian. In active suspensions, obtained by adding artificial swimmers [1] or small microorganisms [2], observations show that the dispersion law remains normal, but the pdf becomes non-Gaussian. We have used concepts of continuous time random walks to model the dispersal and the probability distribution and have obtained good fits to the

observations [3]. In ongoing work we explore the transition to normal dispersal for longer times, and the origin of the trapping that gives rise to the non-normal dispersals.

References

[1] X. Zheng, B. ten Hagen, A. Kaiser, M. Wu, H. Cui, Z. Silber-Li and H. Löwen, *Non-Gaussian statistics for the motion of self-propelled Janus particles: Experiment versus theory*, Phys. Rev. E **88** (2013), 032304.

[2] K.C. Leptos, J.S. Guasto, J.P. Gollub, A.I. Pesci and R.E. Goldstein, *Dynamics of enhanced tracer diffusion in suspensions of swimming eukaryotic microorganisms*, Phys. Rev. Lett. **103** (2009), 198103.

[3] B. Eckhardt and S. Zammert, *Non-normal tracer diffusion from stirring by swimming microorganisms*, Europ. Phys. J. E **35** (2012), 96–97.

Atmospheric coherent structures and aerobiological invasions

Shane D. Ross

(joint work with Amir E. BozorgMagham, David G. Schmale)

Techniques uncovering transport barriers and structures in environmental flows are poised to make a considerable impact on the field of ecology [1, 2]. In particular, Lagrangian coherent structures (LCS) provide a new means for discussion of spatiotemporal characteristics of the passive transport and mixing of atmospheric pathogen populations, paving the way for new management strategies regarding the spread of infectious diseases affecting plants, domestic animals, and humans, including identification of probable source regions and forecasts of regions at high risk. Observations of airborne microorganism using autonomous unmanned aerial vehicles have revealed that 'clouds' of high concentration remain coherent over times of 6–9 hours (determined from auto-correlation of measurements), corresponding to cloud widths of 20–200 km [3]. This time-scale of coherence is in the same range as the time between hyperbolic LCS passages past the sampling location, based on data-assimilated (re-analysis) pastcast wind data [4]. Furthermore, patchiness and abrupt changes in concentration of microbial populations are correlated with hyperbolic LCS passage [5, 4], suggesting that the (a) sampled populations are airborne long enough to be stirred by the atmosphere and (b) hyperbolic LCS play a role in partitioning atmospheric populations into coherent regions over time-scales of < 24 hours [6].

These observations suggest that having reliable forecasts of hyperbolic LCS may contribute to quantitative prediction of microbial concentrations and possible aerobiological invasions. However, chaotic atmospheric dynamics lead to unavoidable forecasting errors in the wind velocity field, which compounds errors in LCS forecasting, imposing certain limits on the forecasting parameters [7]. To obtain more reliable (short-term, < 24 hours) predictions of atmospheric LCS features, we have incorporated two concepts. First is the effect of unresolved turbulent motion; this consideration leads naturally to a stochastic finite-time Lyapunov exponent (SFTLE) field and the resultant stochastic LCS. The second concept is ensemble

FTLE/LCS forecasting using individual members of the ensemble wind field forecasts [8]. We find that the hyperbolic LCS based on a deterministic flow field persist, and in terms of determining source regions for samples, attracting LCS partition the probabilistic source regions into discrete high probability clumps [9].

We consider further notions that may be particularly relevant in an ecological context, such as sampling times which may lead to the most diverse populations (in terms of origins) sampled sequentially at a geographically fixed location [9]. If we consider an n-dimensional ($n = 2, 3$) time-dependent vector field $\mathbf{v}(\mathbf{x}, t)$ over the domain $\mathcal{D} \times \mathcal{T}$ where $\mathcal{D} \subset \mathbb{R}^n$ is the spatial domain and $\mathcal{T}$ is the time-interval of interest, this allows us to define a flow map $\phi : \mathcal{D} \to \mathcal{D}$ which gives the location of the particle seeded at $(\mathbf{x}, t)$ and integrated over a time interval τ (which could be positive or negative), denoted as $\phi_t^\tau(\mathbf{x})$. Consider the curve of particles which were integrated for a time τ since passing through the location $\mathbf{x}$ at time t within the interval $[t_1, t_2]$,

$$S(\mathbf{x}, \tau, t_1, t_2) = \{\phi_t^\tau(\mathbf{x}) \mid t \in [t_1, t_2]\}$$

If $\tau > 0$ ($\tau < 0$) we refer to $S(\mathbf{x}, \tau, t_1, t_2)$ as the destination (source) points, which were released (collected) at point $\mathbf{x}$ at a time t, where t (in the interval $[t_1, t_2]$) parameterizes the release (collection) time. Under certain modest assumptions which hold to a good approximation in geophysical flows, the strain along $S(\mathbf{x}, \tau, t_1, t_2)$ is related to the FTLE, providing a new interpretation of this concept, as well as providing a connection between the local FTLE (the time-series of FTLE at the point $\mathbf{x}$) and the geographic diversity of passive biological samples collected at $\mathbf{x}$ (which correspond to the $\tau < 0$ case where sampling occurs over an interval $[t_1, t_2]$).

References

[1] F. Lekien and S.D. Ross, *The computation of finite-time Lyapunov exponents on unstructured meshes and for non-Euclidean manifolds*, Chaos **20** (2010), 017505.

[2] C. Senatore and S.D. Ross, *Detection and characterization of transport barriers in complex flows via ridge extraction of the finite time Lyapunov exponent field*, Internat. J. Numer. Methods Engrg. **86** (2011), 1163–1174.

[3] B. Lin, A.E. Bozorgmagham, S.D. Ross and D.G. Schmale, *Small fluctuations in the recovery of fusaria across consecutive sampling intervals with unmanned aircraft 100 m above ground level*, Aerobiologia **29** (2013), 45–54.

[4] P. Tallapragada, S.D. Ross and D.G. Schmale, *Lagrangian coherent structures are associated with fluctuations in airborne microbial populations*, Chaos **21** (2011), 033122.

[5] D.G. Schmale, S.D. Ross, T. Fetters, P. Tallapragada, A. Wood-Jones and B. Dingus, *Isolates of Fusarium graminearum collected 40–320 meters above ground level cause Fusarium head blight in wheat and produce trichothecene mycotoxins*, Aerobiologia **28** (2012), 1–11.

[6] P. Tallapragada and S.D. Ross, *A set oriented definition of finite-time Lyapunov exponents and coherent sets*, Commun. Nonlinear Sci. Numer. Simulat. **18** (2013), 1106–1126.

[7] A.E. BozorgMagham, S.D. Ross and D.G. Schmale, *Real-time prediction of atmospheric Lagrangian coherent structures based on forecast data: An application and error analysis*, Physica D **258** (2013), 47–60.

[8] A.E. BozorgMagham and S.D. Ross, *Atmospheric Lagrangian coherent structures considering unresolved turbulence and forecast uncertainty*, submitted.

[9] A.E. BozorgMagham, S.D. Ross and D.G Schmale, *Local finite-time Lyapunov exponent, sampling strategy and probabilistic source regions*, in preparation.

Visualization-oriented comparison of Finite-Time and Finite-Size Lyapunov Exponents

Ronald Peikert

(joint work with Armin Pobitzer, Filip Sadlo, Benjamin Schindler)

The finite-time Lyapunov exponent (FTLE) has become a popular tool in numerical flow visualization [6]. An alternative often used in oceanography is the finite-size Lyapunov exponent (FSLE) [1]. A first direct comparison between FTLE and FSLE was made by Boffetta et al. [2]. They argued that the FTLE is not capable of recognizing the relevant structures, namely the boundaries between chaos and large-scale mixing regime. A recent paper by Karrasch & Haller [4] lists a number of theoretical limitations of FSLE. In Ref. [5] we showed that FTLE and FSLE, if appropriately calibrated, produce comparable results which can be interchangeably used for most purposes in numerical flow visualization. Differences in image quality are mostly due to other factors such as the computational approach, parameter settings, and the sampling rate. In our study a version of FSLE has been used where the initial distance between particle pairs is infinitesimal, in contrast to Aurell's original definition [1], but in accordance with Karrasch's ISLE [4].

Computation of FSLE and FTLE is often based on particle pairs seeded on the nodes of a uniform grid [3], implying a quantization of the range of directions into a set of only four directions. The effect of this is an angle-dependent underestimation of FTLE and FSLE values, leading to visible artifacts in both FTLE and FSLE images, especially if short advection times are used [5]. In principle, quantization effects can be reduced by using a larger set of neighbor particles. However, a better computational approach is to use the Cauchy-Green tensor as an implicit representation of neighbor particles. Its advantage is that no directional quantization occurs, even if gradient estimation is done simply by finite differences using the four grid neighbors. Higher quality gradient estimators can be used if FTLE or FSLE data are generated for a subsequent ridge extraction [7].

FTLE-based visualization depends crucially on the advection time. With increasing advection time the apparent ridges are expected to converge to LCS. In this talk we demonstrate this on two examples of time-periodic analytical velocity fields, where LCS can be determined using the Poincaré map. In a real-world example of a tidal flow, however, we show that short advection times, as compared to the (quasi-)period length, are needed for a meaningful visualization.

As visualization tools, FTLE and FSLE can be seen as dual approaches, both of which are based on the advection time τ and the dispersion factor r. In an FTLE image, τ is a parameter, and r is a dependent variable, while in an FSLE image these roles are swapped. Mapping FTLE or FSLE values monotonically to color indices is equivalent to mapping the dependent variable. Typically, the mapping

is chosen strictly monotonic within an "interesting" subrange and constant outside of it. Under this assumption, we were able to generate highly similar FSLE images, given an FTLE image, and vice versa, by finding the parameter value that maximizes correlation of the pair of (color index) images. Differences still exist, especially for short advection times, and it would be a worthwhile goal to further analyze them. However, we showed that differences are less fundamental than has been suggested in literature.

References

[1] E. Aurell, G. Boffetta, A. Crisanti, G. Paladin and A. Vulpiani, *Growth of noninfinitesimal perturbations in turbulence*, Phys. Rev. Lett. **77** (1996), 1262–1265.

[2] G. Boffetta, G. Lacorata, G. Redaelli and A. Vulpiani, *Detecting barriers to transport: a review of different techniques*, Physica D **159**, 58–70.

[3] I. Hernández-Carracos, C. López, E. Hernández-García and A. Turiel, *How reliable are finite-size Lyapunov exponents for the assessment of ocean dynamics?*, Ocean Modelling **36** (2011), 208–218.

[4] D. Karrasch and G. Haller, *Do Finite-Size Lyapunov Exponents Detect Coherent Structures?*, Chaos **23** (2013), 043126.

[5] R. Peikert, A. Pobitzer, F. Sadlo and B. Schindler, *A Comparison of Finite-Time and Finite-Size Lyapunov Exponents*, In *Topological Methods in Data Analysis and Visualization III*, Springer, 2014.

[6] A. Pobitzer, R. Peikert, R. Fuchs, B. Schindler, A. Kuhn, H. Theisel, K. Matković and H. Hauser, *The State of the Art in Topology-Based Visualization of Unsteady Flow*, Computer Graphics Forum, **30** (2011), 1789–1811.

[7] B. Schindler, R. Peikert, R. Fuchs and H. Theisel, *Ridge Concepts for the Visualization of Lagrangian Coherent Structures*, In *Topological Methods in Data Analysis and Visualization II*, Springer, 2012.

Chaotic advection in a three-dimensional, Ekman-driven eddy

Irina I. Rypina

(joint work with Larry J. Pratt, Tamay M. Özgökmen, Peng Wang, Hank Childs, Yana Bebieva)

Most applications of the dynamical systems approach have been to two-dimensional (2D) or quasi-2D flows, where transport is studied at various depths or isopycnals. Application to 3D flows is challenging, and so examples are rare. We have been working on one such 3D case, investigating chaotic advection in a fully three-dimensional Navier-Stokes flow in a rotating cylinder. This idealization of an isolated ocean eddy is driven from above by a surface stress and has both horizontal swirl and overturning.

In the steady, axially-symmetric flow, each trajectory lives on a torus. These invariant tori, which act as material barriers, start to break when a symmetry-breaking disturbance is added. Both the steady and the time-dependent symmetry-breaking disturbances are considered. Importantly, not all tori are destroyed for moderate values of perturbation; some survive and act as barriers in the perturbed

system. This result is consistent with an extension of the KAM theorem to 3D, volume preserving flows.

Using a combination of high-resolution spectral-element modeling, linear analytical theory, weakly-nonlinear resonance analysis, and a phenomenological model, we explored the behavior of the system over a parameter range appropriate for the ocean mesoscale and *submesoscale*. For shallow eddies the flow was dominated by thin resonant layers sandwiched between unbroken tori, and the stirring rate was weak. Moderately deep eddies had thicker resonant layers, wider-spread chaos and more rapid stirring. This trend reversed for deep eddies, where the vertical rigidity imposed by strong rotation limited the stirring.

Chaos is induced into the flow either by the breakup of the central axis into stable and unstable manifolds in 3d or by resonances. A methodology was derived that describes the resonant condition, the breakup of resonant tori, the geometry of the flow near the resonances, and the resonance widths. This and a version of the KAM theorem are used to interpret our findings.

The results for the steady case can be found in [1]; the analysis of the time-dependent system is currently being written up.

References

[1] L.J. Pratt, I.I. Rypina, T. Ozgokmen, P. Wang, H. Childs and Y. Bebieva, *Chaotic advection in a steady, 3D, Ekman-driven circulation*, J. Fluid Mech. **738** (2014), 143–183.

Estimating long term behavior of flows without trajectory integration: the infinitesimal generator approach

Oliver Junge

(joint work with Gary Froyland, Péter Koltai)

Analysis of the long-term behavior of flows can be broadly classified into geometric methods and statistical methods. Geometrical methods include the determination of fixed points, periodic orbits, and invariant manifolds. Invariant manifolds of fixed points or periodic orbits act as barriers to transport as trajectories may not cross the manifolds transversally. Statistical methods include determining the distribution of points in very long trajectories of a very large set of initial points (i.e. a physical invariant measure [11], often possessing an invariant density) and the identification of meta-stable or almost-invariant sets [3, 5, 4]. Almost-invariant sets partition the phase space into almost dynamically disconnected regions and are important for revealing global dynamical structures that are often invisible to an analysis of trajectories. These metastable dynamics also go under the names of persistent patterns, or strange eigenmodes, both of which are realisable as eigenfunctions of a transfer operator. Frequently, the boundaries of maximally almost-invariant sets (those sets which are locally closest to invariant sets) coincide with certain invariant manifolds [7].

Our focus in the present talk, which subsumes the work of [6], is on statistical methods, although we demonstrate via case studies the relationships to geometrical methods. The most commonly used tool for statistical methods is the transfer operator (or Perron-Frobenius operator). Fixed points of the transfer operator correspond to invariant densities, while eigenfunctions corresponding to real positive eigenvalues strictly less than one provide information on almost-invariant sets. In practice, one typically constructs a finite-rank numerical approximation of a transfer operator and computes large spectral values and eigenfunctions for this finite-rank operator. The construction of the finite-rank approximation requires the integration of many relatively short trajectories with initial points sampled over the domain of the flow. It is this use of *short* trajectories that gives the transfer operator approach additional stability and accuracy when compared with computations based upon very long trajectories. Long trajectories continually accumulate small errors from imperfect numerical integration and finite computer representation of numbers; these small errors quickly grow in chaotic flows. While the transfer operator approach is very stable, it still requires the computation of many small trajectories which can be very time consuming in some systems. The approach we describe in the present work obviates the need for any trajectory integration at all and works directly with the vector field.

Our approach exploits the fact that the evolution of probability densities $u = u(t)$ can be described by generalized solutions of the abstract Cauchy problem $\partial_t u = \mathcal{A}u$. The Perron–Frobenius operator is the evolution operator of this equation, and has the same eigenfunctions as the operator $\mathcal{A}$. The operator $\mathcal{A}$ is an unbounded hyperbolic (if the underlying dynamics is deterministic) or elliptic (if the deterministic dynamics is perturbed by white noise) partial differential operator. Standard techniques allow us to approximate the eigenmodes we are interested in: finite difference, finite volume, finite element and spectral methods yield such discretizations; see [10, 8, 9, 1, 2] and the references therein.

References

[1] J.P. Boyd, *Chebyshev and Fourier Spectral Methods*, Dover Publications, 2001.

[2] C. Canuto, M.V. Hussaini, A. Quarteroni and T.A. Zang, *Spectral methods in fluid dynamics*, Springer, 1991.

[3] M. Dellnitz and O. Junge, *On the approximation of complicated dynamical behavior*, SIAM J. Numer. Anal. **36** (1999), 491–515.

[4] G. Froyland, *Statistically optimal almost-invariant sets*, Physica D **200** (2005), 205–219.

[5] G. Froyland and M. Dellnitz, *Detecting and locating near-optimal almost-invariant sets and cycles*, SIAM J. Sci. Comput. **24** (2003), 1839–1863.

[6] G. Froyland, O. Junge and P. Koltai, *Estimating long term behavior of flows without trajectory integration: the infinitesimal generator approach*, SIAM J. Numer. Anal. **51** (2013), 223–247.

[7] G. Froyland and K. Padberg, *Almost-invariant sets and invariant manifolds – connecting probabilistic and geometric descriptions of coherent structures in flows*, Physica D **238** (2009), 1507–1523.

[8] D. Kröner, *Numerical Schemes for Conservation Laws*, Wiley & Teubner, 1997.

[9] R.J. LeVeque, *Finite Volume Methods for Hyperbolic Problems*, Cambridge University Press, 2002.

[10] A. Quarteroni and A. Valli, *Numerical Approximation of Partial Differential Equations*, Springer, 1994.
[11] L.-S. Young, *What are SRB measures, and which dynamical systems have them?*, J. Statist. Phys. **108** (2002), 733–754.

Set-oriented numerical analysis of time-dependent transport

Kathrin Padberg-Gehle
(joint work with Gary Froyland)

Set-oriented numerical methods involving transfer operators have only recently been recognized as powerful tools for analyzing and quantifying transport processes in time-dependent systems.

The key objects of interest are regions in the phase space of a dynamical system that remain coherent under the dynamics. Almost-invariant sets [1, 2, 3] are spatially fixed regions, while coherent sets [4, 5] move about with minimal dispersion. Almost-invariant and coherent sets can be efficiently identified via Perron-Frobenius operators (or transfer operators). These linear Markov operators can be approximated within a set-oriented framework and subdominant eigenvectors or singular vectors of the resulting stochastic matrices are heuristically used to determine the phase space structures of interest. Most of the previous work addressing optimality criteria for these sets deals with finite-state Markov chains, i.e. discretized transfer operators, and is thus purely finitary. In particular, the crucial role of diffusion is obscured in these descriptions.

Building on recent fundamental work by Froyland [5] we describe a unified functional analytic setting for optimal almost-invariant and coherent set constructions, allowing us to verify the assumptions underlying the finitary framework in [2, 4]. Moreover, we introduce a variation of the coherent set construction that is suited to tracking coherent sets over several finite-time intervals. We discuss the differences and similarities in the mathematical and numerical constructions and explore the role of diffusion, the influence of the finite-time duration and time-directionality. More details can be found in [6].

Transfer operators can also be employed to estimate finite-time expansive behavior along trajectories in autonomous and nonautonomous dynamical systems. Finite-time entropy (FTE) captures nonlinear stretching directly from the entropy growth experienced by a small localised density evolved by the transfer operator. Within the set-oriented approach an approximation of the FTE field is obtained very efficiently and gives similar results to finite-time Lyapunov exponent calculations. The FTE-concept is introduced in [7], see also [8] for related previous work.

References

[1] M. Dellnitz and O. Junge, *On the approximation of complicated dynamical behavior*, SIAM J. Numer. Anal. **36** (1999), 491–515.
[2] G. Froyland, *Statistically optimal almost-invariant sets*, Physica D **200** (2005), 205–219.

[3] G. Froyland and K. Padberg, *Almost-invariant sets and invariant manifolds – connecting probabilistic and geometric descriptions of coherent structures in flows*, Physica D **238** (2009), 1507–1523.
[4] G. Froyland, N. Santitissadeekorn and A. Monahan, *Transport in time-dependent dynamical systems: Finite-time coherent sets*, Chaos **20** (2010), 043116.
[5] G. Froyland, *An analytic framework for identifying finite-time coherent sets in time-dependent dynamical systems*, Physica D **250** (2013), 1–19.
[6] G. Froyland and K. Padberg-Gehle, *Almost-invariant and finite-time coherent sets: directionality, duration, and diffusion*, In *Ergodic Theory, Open Dynamics, and Coherent Structures*, Springer, 2014.
[7] G. Froyland and K. Padberg-Gehle, *Finite-time entropy: a probabilistic approach for measuring nonlinear stretching*, Physica D **241** (2012), 1612–1628.
[8] K. Padberg, B. Thiere, R. Preis and M. Dellnitz, *Local expansion concepts for detecting transport barriers in dynamical systems*, Commun. Nonlinear Sci. Numer. Simulat. **14** (2009), 4176–4190.

Quantifying transport through the relative motion of (almost) coherent sets

Mark A. Stremler
(joint work with Shane Ross, Piyush Grover, Pankaj Kumar, Pradeep Rao)

There is a clear need to understand and predict time-dependent transport in flows with very complex dynamics, such as in the motion of pollutants in the atmosphere and oceans. The identification of various coherent structures, including Lagrangian Coherent Structures (LCS) [6, 9], Finite Time Coherent Sets (FTCS) [4], and Almost Invariant Sets (AIS) [3], is generating important insight regarding the role of dynamical structure in the evolution of complex systems. These approaches give a detailed view of the *spatial complexity* of the dynamics in a system over a finite time window. Determining how this finite-time structure can be pieced together to give information about long-time global behavior of the system can be difficult.

In an alternative approach, the braiding of a small number of trajectories in a flow can give information regarding the *temporal complexity* in the system over long periods of time [1]. The braiding of three or more trajectories can yield a non-zero topological entropy, h, which for C^∞ diffeomorphisms (such as for fluid flow) is equal to the maximal growth rate of smooth arcs under iteration of the flow map [8]. If the trajectories are periodic in time, application of the Thurston-Nielsen Classification Theorem [2, 13] quantifies h based on information from a single period, and Handel's isotopy stability theorem [7] guarantees that this value is a lower bound on h for any isotopic diffeomorphism. The existence of trajectories moving on a *pseudo-Anosov* braid guarantees that non-trivial material lines in at least a portion of the surrounding fluid will experience exponential stretching [1, 12]. Even for aperiodic flows, an ensemble of appropriately chosen trajectories can give a good approximation of the topological entropy [11]. Despite the power of this topology-based approach, however, it cannot give any information about the extent of the spatial complexity in the flow. In the worst-case scenario, the

exponential stretching is restricted to a set of measure zero. Furthermore, it can be challenging to identify the 'correct' trajectories for the analysis [11].

We are exploring the merger of these two points of view: using (almost) coherent sets to identify the spatial complexity of a system over finite time, and using the braiding of trajectories from different (almost) coherent sets to quantify the temporal complexity that comes from the relative motion of these sets. Our initial investigation has focused on exploring a simple time-periodic viscous flow in a two-dimensional lid-driven cavity (LDC). For a range of system parameters, there exist AIS in this flow that periodically interchange position, giving what we refer to as Almost Cyclic Sets (ACS) [10]. Periodically continued trajectories from these ACS generate a pseudo-Anosov braid, predicting that a minimum level of exponential stretching is achieved in some portion of the domain. For viscous flows such as this LDC, it is observed that the resulting chaotic transport covers a significant portion of the domain. Thus, these initial results suggest that there is value in this merged viewpoint.

Identification of ACS comes from considering the eigenspectrum of the Perron-Frobenius operator (PF): the eigenvectors define the spatial extent of the ACS, and the corresponding eigenvalues give a measure of their coherence. Varying the system parameters in the LDC leads to bifurcations in the structure of these eigenvectors [5]. With these bifurcations come changes in the corresponding braid topology, and these different braids predict different minimum bounds on h. These changes in the entropy bounds are clearly reflected in the actual stretching of material lines in the flow [5]. Thus, in this system, bifurcations in the ACS structure correspond well with changes in the underlying topological 'skeleton' of the stirring. It is an open question whether this relationship between bifurcations in the PF eigenspectrum and changes in the entropy of the system holds more generally.

As the structure of the LDC flow becomes more complex, we find that eigenvectors from a given spectrum become more variable in the ACS structure they identify. Including trajectories from ACS identified by multiple eigenvectors tends to increase the accuracy of the lower bound on h. However, at present it is not clear in general how many eigenvectors should be considered in order to achieve sufficient accuracy. An increase in complexity also gives rise to the possibility of aperiodic behavior; a future step for this work will be to use FTCS in identifying braiding trajectories.

References

[1] P. L. Boyland, H. Aref and M. A. Stremler, *Topological fluid mechanics of stirring*, J. Fluid Mech. **403** (2000), 277–304.

[2] A. J. Casson and S. A. Bleiler, *Automorphisms of surfaces after Nielsen and Thurston*, Cambridge University Press, 1988.

[3] M. Dellnitz and O. Junge, *On the approximation of complicated dynamical behavior*, SIAM J. Numer. Anal. **36** (1999), 491–515.

[4] G. Froyland, N. Santitissadeekorn and A. Monahan, *Transport in time-dependent dynamical systems: Finite-time coherent sets*, Chaos **20** (2010), 043116.

[5] P. Grover, S. D. Ross, M. A. Stremler and P. Kumar, *Topological chaos, braiding and bifurcation of almost-cyclic sets*, Chaos **22** (2012), 043135.

[6] G. Haller and F. J. Beron-Vera, *Geodesic theory of transport barriers in two-dimensional flows*, Physica D **241** (2012), 1680–1702.
[7] M. Handel, *Gobal shadowing of pseudo-Anosov homeomorphisms*, Ergodic Theory Dyn. Syst. **5** (1985), 373–377.
[8] S. Newhouse and T. Pignataro, *On the estimation of topological entropy*, J. Stat. Phys. **72** (1993), 1331–1351.
[9] T. Peacock and G. Haller, *Lagrangian coherent structures: The hidden skeleton of fluid flows*, Phys. Today **66** (2013), 41–47.
[10] M. A. Stremler, S. D. Ross, P. Grover and P. Kumar, *Topological chaos and periodic braiding of almost-cyclic sets*, Phys. Rev. Lett. **106** (2011), 114101.
[11] J.-L. Thiffeault, *Braids of entangled particle trajectories*, Chaos **20** (2010), 017516.
[12] J.-L. Thiffeault and M. D. Finn, *Topology, braids and mixing in fluids*, Phil. Trans. R. Soc. A **364** (2006), 3251–3266.
[13] W. P. Thurston, *On the geometry and dynamics of diffeomorphisms of surfaces*, Bull. Amer. Math. Soc. **19** (1988), 417–431.

Biological reactions with coherent structures

Wenbo Tang
(joint work with Christopher Luna, Aditya Drumuntarao)

Coherent structures are ubiquitous in environmental and geophysical flows. They are finite-time entities that inhibit or enhance passive scalar transport over some time interval. Recent advances in the identification of finite-time transport barriers have enabled the extraction of organizing templates for passive scalars in the limit of infinitesimal diffusion.

With finite diffusion, scalars can escape barriers formed by the organizing structures via random walk. Reaction further complicates the system as the scalar quantities also interact and evolve in addition to advection-diffusion. Dynamical systems approach has been shown to be successful in analyzing reaction processes in the infinite-time or time-periodic flow case for open flows. Over finite time, it is unclear how reaction processes can be related to the finite-time entities developed for passive scalars.

A convenient tool to extract finite-time Lagrangian stretching rate is the Finite-Time Lyapunov Exponent (FTLE). Although it has been shown that highlighting features of FTLE field do not necessarily correspond to exponential stretching transverse to the coherent structures, and transport barriers are not directly available just from the FTLE field itself; a quick evaluation of the complexity of the flow field can be revealed. For simple flows, FTLE highlighters (ridges of FTLE or FTLE gradient) typically serve as the effective boundaries for different chaotic mixing behaviors. In [1], we have shown that for a Bickley jet flow, the coherent structures demarcated by the FTLE field give rise to different dispersion statistics when finite diffusion is represented by random walk processes. As such, diffusion processes are similar within similar types of coherent structures.

In this presentation, we show, by using example of an autocatalytic reaction, that reaction processes can also be tied to finite-time measures of the Lagrangian stretching rate, which varies quite significantly in different types of flow topologies.

In particular, we consider the Fisher-Kolmogorov-Petrovsky-Piskunov (FKPP) equation embedded in a flow with two oscillating gyres. In this setting, there is only one stable state of the system, where the reacting scalar field saturates to the carrying capacity specified by the FKPP reaction. However, we show that the finite-time reaction, in terms of the variability of the average scalar concentration at finite-time, is intimately related to the FTLE field. In fact, it is the early-stage advection-diffusion-reaction that sets the scalars into different effective reaction rates. Over long time, the scalar bulk reaction rate falls onto the same curve (with cases of different starting disturbances reaching that curve at different times). The reaction process can be separated into four different stages, and a model for the evolution of effective reaction can be constructed based on these stages. We show that the model based on FTLE represents the variabilities from the actual simulations well.

With autocatalytic reaction, only one stable state exists, and hence the long-term scalar behavior is trivial. In our very recent study, we show that, when two stable states from a bi-stable reaction process is placed together, flow structures can serve as the incubator for certain states—with small disturbances released in high-stretching, stochastic regions, the disturbances quickly homogenize with the ambient, where the system asymptotes. As comparison, for small disturbances released within transport barriers, the coherent structures serve as incubators for the disturbance state, and over significantly long time, the scalar field can asymptote to the disturbance state. This highlights the importance of flow topology on diffusion-reaction processes.

References

[1] W. Tang and P. Walker, *Finite-time statistics of scalar diffusion in Lagrangian coherent structures*, Phys. Rev. E **86** (2012), 045201(R).

[2] W. Tang and C. Luna, *Dependence of advection-diffusion-reaction on flow coherent structures*, Phys. Fluids **25** (2013), 105602.

A new concept of local metric entropy for finite-time nonautonomous dynamical systems

Stefan Siegmund

(joint work with Luu Hoang Duc)

Let $J \subset \mathbb{R}$ be compact and $(X(t))_{t\in J} \subseteq \mathbb{R}^n$ be a family of subsets of $\mathbb{R}^n$ indexed by J. Then $X := \{(t,x) \in J \times \mathbb{R}^n : x \in X(t)\}$ is a (trivial) fibre bundle over the base space J. We write $|J| := \max J - \min J$. A continuous map $\varphi\colon J \times X \to X$ is called a *finite-time nonautonomous dynamical system (FTNDS) on X over J*, if for $t,u,s \in J$ and $x \in X(s)$ the properties $\varphi(s,s,x) = (s,x)$ and $\varphi(t,u,\varphi(u,s,x)) = (t,\varphi(t,s,x))$ hold. For ease of notation we identify φ with the two-parameter family of maps $\varphi(t,s) = \varphi(t,s,\cdot)\colon X(s) \to X(t) \subseteq \mathbb{R}^n$, $t,s \in J$, and the defining properties read as

$$\varphi(s,s)x = x \quad \text{and} \quad \varphi(t,u) \circ \varphi(u,s)x = \varphi(t,s)x.$$

Let φ be an FTNDS on X over J and $\gamma \in \mathbb{R}$. The *finite-time metric entropy (FTME)* with weight γ at $(t_0, x_0) \in X$ is defined by

$$h^\gamma_{t_0}(x_0) \coloneqq \lim_{\varepsilon \to 0} h^\gamma_{t_0}(x_0, \varepsilon), \qquad \text{with} \qquad h^\gamma_{t_0}(x_0, \varepsilon) \coloneqq -\frac{1}{|J|} \log \frac{\mu\big(B^\gamma_{t_0}(x_0, \varepsilon)\big)}{\mu\big(B(x_0, \varepsilon)\big)},$$

where the orbit neighborhood $B^\gamma_{t_0}(x_0, \varepsilon)$ is defined for $(t_0, x_0) \in X, \varepsilon \geq 0$ by

$$B^\gamma_{t_0}(x_0, \varepsilon) \coloneqq \left\{ x \in X(t_0) \colon \sup_{t \in J} \|\varphi(t, t_0)x - \varphi(t, t_0)x_0\| \, \mathrm{e}^{-\gamma(t - t_0)} \leq \varepsilon \right\}.$$

Our concept of FTME is different from the probabilistic concept of finite-time entropy (FTE) introduced by Froyland and Padberg-Gehle [1] which is based on a smoothed transfer operator.

We prove a finite-time version of Pesin's entropy formula [4] by relating the FTME to the sum of all *finite-time Lyapunov exponents* (FTLE) $\lambda_i(t_0, x_0, T)$, $i = 1, \ldots, n$, which are not less than γ. More precisely, for $x_0 \in X(t_0)$, the finite-time version of Pesin's entropy formula states that

$$0 \leq \sum_{i=1}^{n} \big(\lambda_i(t_0, x_0, T) - \gamma\big)^+ - h^\gamma_{t_0}(x_0) \leq \frac{n \log 2 + \log \Gamma(\frac{n}{2} + 1) - \frac{n}{2} \log \pi}{T}$$

where $a^+ = \max\{a, 0\}$ and $J = \{0, T\}$ for $T > 0$.

FTME can be expressed in terms of Lyapunov exponents and is frame-independent in the sense of Haller (see [2] and the references therein). We show that for autonomous differential equations

$$\dot{x} = f(x), \qquad t \in [0, T], \ x \in U \subseteq \mathbb{R}^n,$$

with C^2 function $f \colon U \to \mathbb{R}^n$ and $T > 0$, the frame-dependent, weighted FTME field

(1)

$$x \mapsto H(x) \coloneqq h^{\gamma(x, T, f(x))}(x), \qquad \text{with} \quad \gamma(x, T, f(x)) = \frac{1}{T} \log \frac{\|f(\varphi(T, 0, x))\|}{\|f(x)\|},$$

exhibits ridge and trough-like coherent structures which approach classical invariant manifolds as $T \to \infty$. The weight $\gamma(x, T, f(x))$ measures the exponential stretching along the vector field. See Figs. 1 and 2, which were produced by Tino Weinkauf (with integration time $T = 2$) during the workshop.

References

[1] G. Froyland, K. Padberg-Gehle, *Finite-time entropy: a probabilistic approach for measuring nonlinear stretching*, Physica D **241** (2012), 1612–1628.

[2] G. Haller, *A variational theory of hyperbolic Lagrangian coherent structures*, Physica D **240** (2011), 574–598.

[3] L.H. Duc, S. Siegmund, *A new concept of local metric entropy for finite-time nonautonomous dynamical systems*, preprint, available from `arxiv.org/abs/1401.6664`.

[4] Ya. Pesin, *Characteristic Lyapunov exponents and smooth ergodic theory*, Russ. Math. Surveys **32** (1977), 55–114.

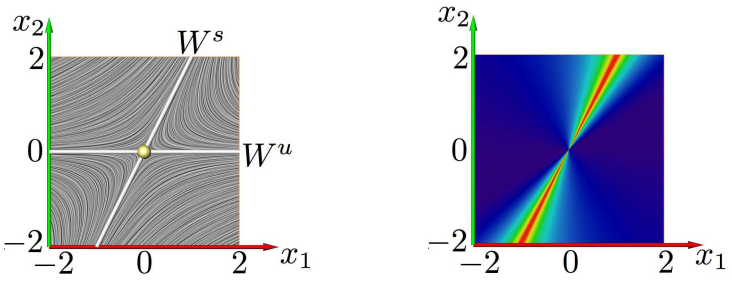

FIGURE 1. Vector field, invariant manifolds (left) and weighted FTME field (1) for $\dot{x}_1 = x_1 - x_2$, $\dot{x}_2 = -x_2$ (blue $\simeq 0$, red $\simeq 1$).

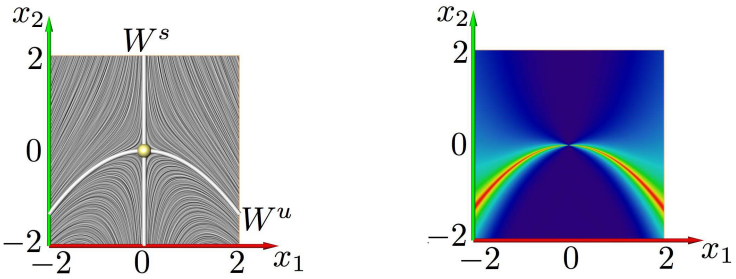

FIGURE 2. Vector field, invariant manifolds (left) and weighted FTME field (1) for $\dot{x}_1 = -x_1$, $\dot{x}_2 = x_1^2 + x_2$ (blue $\simeq 0$, red $\simeq 2.25$).

Classifying Lagrangian fluxing particles through a fixed curve for non-autonomous flows: Theory and applications

QINGHAI ZHANG

The uniqueness of the solution of an nonautonomous ODE $\frac{\mathrm{d}\mathbf{x}}{\mathrm{d}t} = \mathbf{u}(\mathbf{x}, t)$ admits a flow map $\phi\colon \mathbb{R}^{\mathrm{D}} \times \mathbb{R} \times \mathbb{R} \to \mathbb{R}^{\mathrm{D}}$ that maps the initial position $p(t_0)$ of a Lagrangian particle p, the initial time t_0, and the time increment τ to $p(t_0 + \tau)$, the position of p at time $t_0 + \tau$. The shorthand notations $\overrightarrow{p} = \phi_{t_0}^{\tau}(p_0)$ and $\overleftarrow{p} = \phi_{t_0+\tau}^{-\tau}(p(t_0 + \tau))$ are used if t_0 and τ are clear from the context. One well-known characteristic curve of the flow map is a *pathline*, $\Phi_{t_0}^{\pm k}(p) \coloneqq \left\{\phi_{t_0}^{\pm\tau}(p) : \ \tau \in (0, k)\right\}$. In comparison, a *backward streakline* [2] is the loci of all particles that will pass continuously through a fixed seeding location M,

$$\Psi_{t_0}^{-k}(M) \coloneqq \left\{\phi_{t_0-k+\tau}^{-\tau}(M) : \ \tau \in (0, k)\right\}.$$

where the time increment $k > 0$.

A *fluxing particle* to a fixed simple curve $\widetilde{LN}$ over the time interval $(t_0, t_0 + k)$ is a particle p whose pathline $\Phi_{t_0}^{+k}(p)$ *properly* intersects $\widetilde{LN}$ at least once. The *sign of an intersection* $(\mathbf{x}_I, t_I)$ is defined as $\mathsf{S}_I = \operatorname{sgn}(\mathbf{n}_{\widetilde{LN}}(\mathbf{x}_I) \cdot \mathbf{u}(\mathbf{x}_I, t_I))$ where $\mathbf{n}_{\widetilde{LN}}$ is the unit normal of $\widetilde{LN}$; it determines the type of the flux as an *out-flux* if $\mathsf{S}_I = +1$, or an *in-flux* if $\mathsf{S}_I = -1$. The *fluxing index* of a fluxing particle is the sum of the signs of all the intersections. The *flux set of index* n through a simple

curve $\widetilde{LN}$ over (t_0, t_0+k), denoted $\mathcal{F}^n_{\widetilde{LN}}(t_0,k)$, is the point set of all the fluxing particles of index n at time t_0.

Given a fixed simple curve $\widetilde{LN}$, a velocity field, and a time interval (t_0, t_0+k), the fluxing index defines an equivalence class on the points of the plane. Clearly the flux sets $\mathcal{F}^n_{\widetilde{LN}}(t_0,k)$ with $n \in \mathbb{Z}$ are pairwise disjoint and partition $\mathbb{R}^2$. The rest of this report concerns the explicit construction of the flux sets.

The *winding number of an oriented closed curve γ around a point*[1] $\mathbf{x} \in \mathbb{R}^2 \setminus \gamma$ is the number

$$w_\gamma(\mathbf{x}) \coloneqq \frac{\theta(1)-\theta(0)}{2\pi},$$

where $\theta\colon [0,1] \to \mathbb{R}$ is the continuous function as the angle of $\gamma(t)$ in the polar coordinate system whose pole is at $\mathbf{x}$, i.e. $\gamma(t) = \mathbf{x} + \rho(t)\,(\cos\theta(t),\ \sin\theta(t))$.

The *winding region* (WR) $\mathcal{W}_\gamma$ associated with an oriented closed planar curve γ is

$$\mathcal{W}_\gamma \coloneqq \bigcup_{n\in\mathbb{Z}\setminus\{0\}} \mathcal{W}^n_\gamma, \qquad\qquad \mathcal{W}^n_\gamma \coloneqq \left\{\mathbf{x}\in\mathbb{R}^2 : w_\gamma(\mathbf{x}) = n\right\},$$

where $\mathcal{W}^n_\gamma$ is the *WR of index n*.

In [2], the donating region of a fixed simple open curve $\widetilde{LN}$ is constructed by its preimage and the backward streaklines seeded at L and N. The following definition generalizes this notion using WRs.

Definition 1 (Generalized donating regions)**.** For a given velocity field $\mathbf{u}(\mathbf{x},t)$, the *donating region* (DR) associated with a simple open curve $\widetilde{LN}$ over the time interval (t_0, t_0+k) is the WR of a closed curve $\gamma_{\mathcal{D}}$,

$$\begin{aligned}
&\mathcal{D}_{\widetilde{LN}}(t_0,k) \coloneqq \mathcal{W}_{\gamma_{\mathcal{D}}},\\
&\gamma_{\mathcal{D}} \coloneqq L \cup \widetilde{LN} \cup N \cup \Psi^{-k}_{t_0+k}(N) \cup \overleftarrow{N} \cup \phi^{-k}_{t_0+k}\left(\widetilde{NL}\right) \cup \overleftarrow{L} \cup \Psi^{-k}_{t_0+k}(L),
\end{aligned}$$

where $\gamma_{\mathcal{D}}$ is called the *generating curve* of the DR and is oriented by the closed vertex sequence $L \to N \to \overleftarrow{N} \to \overleftarrow{L} \to L$. Also, $\mathcal{D}^n_{\widetilde{LN}}(t_0,k) \coloneqq \mathcal{W}^n_{\gamma_{\mathcal{D}}}$.

A DR $\mathcal{D}_{\widetilde{LN}}(t_0,k)$ is *normal* if the backward streaklines $\Psi^{-k}_{t_0+k}(L)$ and $\Psi^{-k}_{t_0+k}(N)$ neither self-intersect nor intersect each other. As a key observation, the set of loops $\left\{\gamma_{\mathcal{D}_{\widetilde{LN}}(t_0+\tau,k-\tau)} : \tau\in[0,k]\right\}$ is a homotopy class, which, together with the Hopf theorem, eventually leads to the equivalence of DRs to flux sets [1].

Theorem 1 (Generalized DRs in two dimensions)**.** *A normal DR of a simple open curve $\widetilde{LN}$ is index-by-index equivalent to the flux set of $\widetilde{LN}$,*

$$\mathcal{D}^n_{\widetilde{LN}}(t_0,k) = \mathcal{F}^n_{\widetilde{LN}}(t_0,k), \qquad \forall n\in\mathbb{Z},$$

[1]The winding number of γ around a point $\mathbf{x}\in\gamma$ can be defined appropriately so that the DRs $\mathcal{D}^n_{\widetilde{LN}}(t_0,k)$'s in Definition 1 satisfies Theorem 1 and form a pairwise disjoint partition of $\mathbb{R}^2$. It can also be generalized to higher-dimensional spaces; see [1].

where $\mathbf{n}_{\widetilde{LN}}$ *is chosen to be the outward unit normal of* $\mathcal{D}^+_{\widetilde{LN}}$ *or the inward unit normal of* $\mathcal{D}^-_{\widetilde{LN}}$.

A scalar function f is a *conserved scalar* of $\mathbf{u}$ if, for any $\tau \in \mathbb{R}$,

$$\frac{\mathrm{d}}{\mathrm{d}\tau} \int_{\phi^\tau_{t_0}(\mathcal{M})} f(\mathbf{x}, t_0 + \tau) \mathrm{d}\mathbf{x} = 0, \tag{1}$$

where t_0 is a fixed time and $\mathcal{M}$ a fixed compact manifold with boundaries. The Reynolds transport theorem then leads to flux identities [1] as follows:

Theorem 2 (DR flux identities[2])**.** *Let* $\widetilde{LN}$ *be a fixed simple open curve whose* C^1 *discontinuities form a set of measure zero. If a scalar function* f *satisfies* (1) *and the DR* $\mathcal{D}_{\widetilde{LN}}(t_0, k)$ *is normal, then*

$$\int_{t_0}^{t_0+k} \int_{\widetilde{LN}} f\, \mathbf{u} \cdot \mathbf{n}_{\widetilde{LN}} \,\mathrm{d}s\,\mathrm{d}t = \sum_{n\in\mathbb{Z}} |n| \int_{\mathcal{D}^n_{\widetilde{LN}}(t_0,k)} f(\mathbf{x}, t_0) \mathrm{d}\mathbf{x}.$$

The above theorem states that the flux through a fixed curve during the interval $(t_0, t_0 + k)$ can be converted to an integral at the initial time t_0. It has a number of applications in numerical PDEs and multiphase-flow simulations; see [3] and [4] for two examples.

References

[1] Q. Zhang, *Classifying Fluxing particles through a fixed curve for scalar conservation laws*, submitted.

[2] Q. Zhang, *On Donating Regions: Lagrangian Flux through a Fixed Curve*, SIAM Review **55** (2013), 443–461.

[3] Q. Zhang, *Highly Accurate Lagrangian Flux Calculation via Algebraic Quadratures on Spline-Approximated Donating Regions*, Comput. Methods Appl. Mech. Engrg. **264** (2013), 191–204.

[4] Q. Zhang, *On a family of unsplit advection algorithms for volume-of-fluid methods*, SIAM J. Numer. Anal. **51** (2013), 2822-2850.

Propagation barriers for fronts in fluid media with general time-dependence

Kevin Mitchell

(joint work with John Mahoney)

The passive advection of inert particles in fluid flows is important both for its direct relevance to fluid mixing and for its broader connection to Hamiltonian dynamics and chaos. Here, we consider the generalization of advective transport to "active" media, specifically to media that support some kind of front propagation: for example, the expansion of chemical reaction fronts in microfluidic mixers, plankton blooms in large-scale oceanic flows, phase transitions in liquid crystals,

[2]This is a generalization of [2, Theorem 4.11]

or even the spread of disease within a mixing population. We have been particularly motivated by recent table-top experiments of chemical reaction (Belasov-Zabotinsky) fronts propagating through magnetohydrodynamically driven quasi-two-dimensional flows [1, 2, 3, 4, 5]. This laboratory system has demonstrated a range of complex dynamical phenomena, from percolation-type behavior, to the locking of the reaction profile to periodic driving, to pinning of reaction fronts to fluid vortices.

Previously, a three-dimensional dynamical systems model was used to analyze the propagation of individual front elements [6, 7, 8]. In terms of the (x, y) position of a front element and the orientation angle θ of the tangent to the front, one finds

$$\begin{aligned} \dot{x} &= u_x + v_0 \sin\theta, \\ \dot{y} &= u_y - v_0 \cos\theta, \\ \dot{\theta} &= -u_{x,x} \sin\theta\cos\theta - u_{x,y}\sin^2\theta + u_{y,x}\cos^2\theta + u_{y,y}\sin\theta\cos\theta, \end{aligned} \tag{1}$$

where (u_x, u_y) is the fluid velocity field and v_0 is the front propagation speed in the local fluid frame. The invariant manifolds of this system, called burning invariant manifolds (BIMs), are important, robust, one-sided barriers to front propagation in time-independent or periodically driven flows. BIMs play a central role in guiding the propagating fronts through the medium, determining the patterns formed by the fronts, and providing a theoretical foundation to explain many of the observed laboratory phenomena.

Historically, the application of invariant manifold theory was restricted to time-periodic flows. More recently, however, the study of Lagrangian Coherent Structures (LCS) have greatly extended the applicability of invariant manifold techniques to the general case of aperiodic, and even turbulent, flows [9, 10]. Over the past decade, interest in LCS techniques has blossomed across a wide range of applications [11]. Motivated by these developments, we demonstrate here that LCS techniques can be adapted to construct the most relevant (one-sided) barriers to front propagation in flows with general time dependence. Our approach follows the recent work of Farazmand, Blazevski, and Haller [12], in which transport barriers were characterized as curves of minimal Lagrangian shear.

Following [12], we obtain a one-sided hyperbolic barrier $\mathbf{r}(\tau)$ to front propagation, described as a curve of zero Lagrangian shear, satisfying $\langle d\mathbf{r}/d\tau, D\ d\mathbf{r}/d\tau\rangle = 0$, where

$$D(\mathbf{r},\theta) = \frac{1}{2}(C(\mathbf{r},\theta)\Omega - \Omega C(\mathbf{r},\theta)), \quad \Omega = \begin{pmatrix} 0 & -1 \\ 1 & 0 \end{pmatrix}, \tag{2}$$

and where

$$C(\mathbf{r},\theta) = \Pi_{xy}(\nabla F)^T \Pi_{xy}(\nabla F)\Pi_{xy}$$

is the "projected" Cauchy-Green strain tensor; Π_{xy} is the projection from the $xy\theta$ tangent-space to the xy tangent-space, and ∇F is the three-by-three gradient tensor of the map F defined as the time evolution of Eq. (1) over the time interval of interest. Among the shearless curves satisfying (2), the *burning* Lagrangian coherent structure (BLCS) is the one maximizing the compression along the curve.

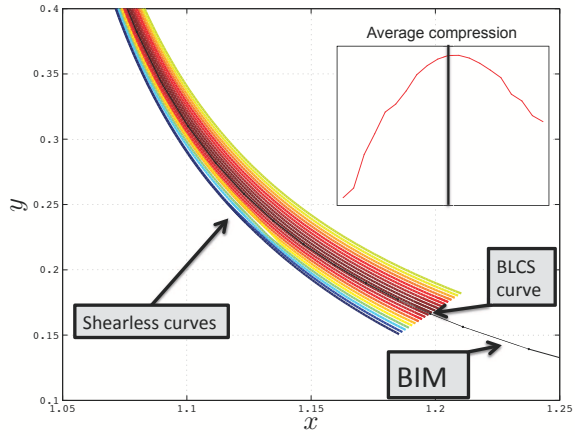

FIGURE 1. Shearless curves for a time-independent flow are shown in color. The BIM is shown in black. The BLCS curve, which maximizes the compression (inset), lies very near the BIM.

As an example, Fig. 1 shows the shearless curves satisfying Eq. (2) for a time-independent alternating vortex flow. The burning invariant manifold (BIM) is shown for reference. The BLCS is the shearless curve maximizing the average compression. Notice that the BLCS follows the BIM very closely, providing validation of our construction.

REFERENCES

[1] M.S. Paoletti and T.H. Solomon, *Experimental studies of front propagation and mode-locking in an advection-reaction-diffusion system*, Europhys. Lett. **69** (2005), 819–825.
[2] M.S. Paoletti, C.R. Nugent and T.H. Solomon, *Synchronization of oscillating reactions in an extended fluid system*, Phys. Rev. Lett. **96** (2006), 124101.
[3] J.R. Boehmer and T.H. Solomon, *Fronts and trigger wave patterns in an array of oscillating vortices*, EPL **83** (2008), 58002.
[4] M.E. Schwartz and T.H. Solomon, *Chemical reaction fronts in ordered and disordered cellular flows with opposing winds*, Phys. Rev. Lett. **100** (2008), 028302.
[5] D. Bargteil and T. Solomon, *Barriers to front propagation in ordered and disordered vortex flows*, Chaos **22** (2012), 037103.
[6] J. Mahoney, D. Bargteil, M. Kingsbury, K. Mitchell and T. Solomon, *Invariant barriers to reactive front propagation in fluid flows*, EPL **98** (2012), 44005.
[7] K.A. Mitchell and J. Mahoney, *Invariant manifolds and the geometry of front propagation in fluid flows*, Chaos **22** (2012), 037104.
[8] J.R. Mahoney and K.A. Mitchell, *A turnstile mechanism for fronts propagating in fluid flows*, Chaos **23** (2013), 043106.
[9] G. Haller and F. J. Beron-Vera, *Geodesic theory of transport barriers in two-dimensional flows*, Physica D **241** (2012), 1680–1702.
[10] S.C. Shadden, F. Lekien and J.E. Marsden, *Definition and properties of Lagrangian coherent structures from finite-time Lyapunov exponents in two-dimensional aperiodic flows*, Physica D **212** (2005), 271–304.
[11] *Focus Issue: Lagrangian Coherent Structures in Fluid Flows*, Chaos **20** (2010).
[12] M. Farazmand, D. Blazevski and G. Haller, *Shearless transport barriers in unsteady two-dimensional flows and maps*, submitted preprint, available from `arxiv.org/abs/1308.6136`.

Path lengths in turbulence

Nicholas T. Ouellette
(joint work with Haitao Xu, Eberhard Bodenschatz)

Although there is still no general consensus on the optimal definition of a "coherent structure" in highly unsteady flows, nearly all structure-detection tools and algorithms require knowledge of the flow velocity field. In many situations, however, and particularly for the case of high-Reynolds-number turbulence experiments, this information is not available. Instead, experiments tend to resolve either snapshots of slices of the velocity field, such as a single two-dimensional plane embedded in the full three-dimensional flow, or the time-resolved trajectories of a small number of fluid elements that sparsely sample the flow field. Neither traditional nor modern analysis tools are therefore readily applicable to experimental turbulence data sets.

It is widely thought that high-aspect ratio, highly rotational structures play a significant role in turbulent intermittency. The notion of these "vortex worms" has been invoked to explain various anomalous features of turbulence statistics, particularly in the Lagrangian framework [1, 2]. If such structures indeed exist and play an important role in the Lagrangian dynamics of the flow, their signature should be measurable in the geometric properties of particle trajectories: for a fluid element caught on a rapidly rotating coherent vortex, the distance travelled by the particle in time ought to grow in a different fashion from its displacement from its initial position.

To look for this effect, we recorded the trajectories of tracer particles moving in a highly turbulent experimental water flow between counter-rotating disks. We measured the statistics of both the arc length S of the trajectories and the displacement R as a function of time [3]. Although both $\langle S^2 \rangle$ and $\langle R^2 \rangle$ scale as t^2, their difference reveals sub-leading terms: we find that $\langle S^2 - R^2 \rangle \sim t^3$. But we can construct the difference of these two terms in a different way by including the covariance $\langle SR \rangle$, and, surprisingly, we find that $\langle (S - R)^2 \rangle \sim t^{3.7}$. We know of no theoretical argument that can explain these exponents, but suggest that they may be related to nontrivial structure in the flow field. Explaining these unusual scalings may lead to new ways of characterizing the link between flow structure and turbulence statistics.

References

[1] L. Biferale, G. Boffetta, A. Celani, A. Lanotte, and F. Toschi, *Particle trapping in three-dimensional fully developed turbulence*, Phys. Fluids **17** (2005), 021701.

[2] J. Bec, L. Biferale, M. Cencini, A. S. Lanotte, and F. Toschi, *Effects of vortex filaments on the velocity of tracers and heavy particles in turbulence*, Phys. Fluids **18** (2006), 081702.

[3] N. T. Ouellette, E. Bodenschatz, and H. Xu, *Path lengths in turbulence*, J. Stat. Phys. **145** (2011), 93–101.

Flow barriers in realistic flows, and their relationship to invariant manifolds

Sanjeeva Balasuriya

Unambiguously identifying time-varying flow barriers in realistic unsteady flows faces many difficulties, since velocity fields are usually only available as spatially and temporally discrete data over a finite time. Despite a lack of agreement on the *definition* of flow barriers, a variety of methods for locating them are in usage. These include—but are not limited to—passively advecting tracers; Finite-Time Lyapunov Exponents; eigen/singular-vectors of transfer operators; complexity measures along trajectories; curves/surfaces of extremal stretching, or shearing, or flux, or attraction; ergodic quotient; and topological entropy. Interesting theoretical and computationally-efficient advances are being made at a rapid rate within the context of each proposed method of identifying flow barriers, as were explored by the many specialists attending this workshop.

Flow barrier detection: As more and more instances of these methods being applied to oceanographic, atmospheric and experimental data are being reported, it would be good to be certain of the legitimacy of the conclusions reached in such studies. As such, several broad questions are of concern:

1. *In what way are these definitions related to each other?* How is a curve of extremal deformation related to eigenfunctions of the transfer operator? Is a mesohyperbolic trajectory associated with an extremal flux? Questions of this sort can be posed between any two definitions, and demand our attention.

2. *What is the accuracy of each definition in identifying flow barriers?* Strangely, there is little analysis of this crucial question. While there is an obvious disincentive for a proponent of a particular definition to undertake such an investigation, this is surely scientifically necessary. A major problem in analysing this is having unequivocal unsteady flow barriers with which to compare.

3. *And what is a flow barrier in an unsteady flow anyway?* There are simple counter-examples which show that entities across which there is minimal (or zero) flux is a bad definition for this—but what is a flow barrier if it is not some entity associated with minimal transport across it? Should one of the proposed definitions—say a curve/surface of extremal stretching [10]—be used as *the* definition? This is unlikely to hold water, since competing definitions will surely vie for this, and more and more definitions are being developed thick and fast! Are there any features which are *essential* for a flow barrier to possess? For example:

4. *Is frame invariance necessary?* Not all methods for locating supposed flow barriers are frame invariant. A continuing debate on this issue is necessary. If, say, the boundary of an oceanic eddy is identified using some method based on observations from the earth's frame of reference, would the *same* boundary be identified from the reference frame of a ship travelling alongside it? Alternatively, if we want to quantify transport in our frame of reference, do we care what result we get in another frame of reference?

5. *In what sense is time-periodicity implicit in some definitions?* Real flows are patently *not* time-periodic, and thus recent methods that are being used and

developed ostensibly avoid this restriction. However, consider the standard finite-time approach of defining a flow map P from a time t_1 to another time t_2. As an example, suppose the fact that all eigenvalues of a fixed point a of P are within the unit circle is used to argue the stability of a. This argument relies on $P^n(x) \to a$ as $n \to \infty$ for x near a, i.e., repeated applications of P. As a second example, suppose spectral—say, Koopman—methods based on Fourier series on $[t_1, t_2]$ are used. In both examples, the flow has been implicitly assumed time-periodic.

6. *Is the time-variation captured?* Flow barriers in unsteady flows must vary with time. If we think of t_1 and t_2 above as *fixed*, we are simply addressing the limited problem of just *one* iteration of an autonomous map P, thereby ignoring the time-dependence of flow barriers. For a definition/theory to be legitimate and useful, it must genuinely incorporate the time-varying nature; it should quite naturally be able to think of t_2 as a varying entity. Thus, addressing objects like P's invariant sets is surely meaningless in a time-varying setting.

Stable and unstable manifolds: Our initial ideas of flow barriers possibly arose from stable and unstable manifolds of stagnation points in steady flows, which indubitably form flow separators between regions of distinct fluid motion. The clear analogue in *unsteady* flows would be stable and unstable manifolds of hyperbolic trajectories/sets. The trouble is that to define these, one needs *infinite-time* flows. Thus, for an understanding of unsteady flow barriers and associated transport, further developments are called for:

a. *Develop theory of finite-time invariant manifolds:* There are some developments in this regard [12, 7, 8, 13, 9, 15], but theory to specifically locate finite-time flow barriers, and to establish connections with any diagnostic method, would be of tremendous value.

b. *Quantify flux across intersection/non-intersecting invariant manifolds:* While a segment of stable manifold might be considered a transport barrier, since such a segment by itself does not partition space, its location relative to other manifold segments controls how fluid is transported. In nonautonomous flows, this picture is changing with time, and moreover stable and unstable manifolds can intersect in an arbitrary fashion. How do such intersections—or lack of such—lead to transport? For time-periodic flows, transport across a flow barrier composed from such manifold segments can be quantified [14, 1]. For time-aperiodicity, a gate-surface idea [11] can be used to quantify time-dependent transport for nonautonomously *perturbed* 2D flows [2], but a general theory for more realistic flows is lacking. Since when we think of flow *barriers*, there is clearly an intuition regarding lack of transport across these, the development of theory to *quantify* transport explicitly across flow barriers in unsteady flows is highly relevant.

c. *Test models with known invariant manifolds:* There are unsteady nonchaotic models in 2D and 3D in which time-varying stable and unstable manifolds are explicitly known [4]; these apply also to finite time, and their construction explicitly addresses frame-dependence. Segments of invariant manifolds in nonautonomously perturbed chaotic 2D flows can also be computed to leading-order using recent theory [3]. In an alternative approach, recent work [5, 6] enables the determination

of the control velocity needed to force segments of [un]stable manifolds and hyperbolic trajectories to almost follow user-specified time-aperiodic behaviour. Given the explicit nature of all of these models, they offer yet-to-be-exploited opportunities for testing accuracies of different methods of barrier detection.

In summary: Given the unequivocal nature of invariant manifolds as intuitive flow barriers in unsteady flows, their further development towards less idealised flows should be an important avenue we should pursue. These will further assist in the essential task of evaluating the accuracy of the multitudinous diagnostic methods in usage.

References

[1] S. Balasuriya, *Direct chaotic flux quantification in perturbed planar flows: General time-periodicity*, SIAM J. Appl. Dyn. Sys. **4** (2005), 282–311.

[2] S. Balasuriya, *Cross-separatrix flux in time-aperiodic and time-impulsive flows*, Nonlinearity **19** (2006), 2775–2795.

[3] S. Balasuriya, *A tangential displacement theory for locating perturbed saddles and their manifolds*, SIAM J. Appl. Dyn. Sys. **10** (2011), 1100–1126.

[4] S. Balasuriya, *Explicit invariant manifolds and specialised trajectories in a class of unsteady flows*, Phys. Fluids **24** (2012), 127101.

[5] S. Balasuriya and K. Padberg-Gehle, *Controlling the unsteady analogue of saddle stagnation points*, SIAM J. Appl. Math. **73** (2013), 1038–1057.

[6] S. Balasuriya and K. Padberg-Gehle, *Nonautonomous control of stable and unstable manifolds in two-dimensional flows*, submitted.

[7] A. Berger, *On finite-time hyperbolicity*, Commun. Pure Appl. Anal. **10** (2011), 963–981.

[8] L.H. Duc and S. Siegmund, *Hyperbolicity and invariant manifolds for planar nonautonomous systems on finite time intervals*, Intern. J. Bifurc. Chaos, **18** (2008), 641–673.

[9] P. Giesl and M. Rasmussen, *Areas of attraction for nonautonomous differential equations on finite time intervals*, J. Math. Anal. Appl. **390** (2012), 27–46.

[10] G. Haller and F.J. Beron-Vera, *Geodesic theory of transport barriers in two-dimensional flows*, Physica D **241** (2012), 1680–1702.

[11] G. Haller and A. Poje, *Finite time transport in aperiodic flows*, Physica D **119** (1998), 352–380.

[12] D. Karrasch, *Linearization of hyperbolic finite-time processes*, J. Differ. Equ. **254** (2013), 256–282.

[13] M. Rasmussen, *Finite-time attractivity and bifurcation for nonautonomous differential equations*, Differ. Equ. Dyn. Syst. **18** (2010), 57–78.

[14] V. Rom-Kedar, A. Leonard and S. Wiggins, *An analytical study of transport, mixing and chaos in an unsteady vortical flow*, J. Fluid Mech. **214** (1990), 347–394.

[15] B. Sandstede, C.K.R.T. Jones and S. Balasuriya, *Melnikov theory for finite-time vector fields*, Nonlinearity, **13** (2000), 1357–1377.

The impact of windage on the structure of material transport at the ocean surface

Thomas Peacock

Transport of material at the ocean surface plays a crucial role in many environmental processes, from determining the fate of oil slicks to impacting the spawning, calcification and thermal bleaching of coral reefs. Uncertainty surrounding the

outcome of recent disasters, such as the Deepwater Horizon oil spill and the debris distribution resulting from the Tohoku tsunami, emphasizes the pressing need for improved analysis and prediction tools, but it is a substantial challenge to interpret the intricate tangle of particle trajectories that typically arises for the spatiotemporally complex flows of the energetic ocean surface.

Recently, the method of Lagrangian Coherent Structures (LCS) has demonstrated clear potential for providing both insight and predictability based on uncovering the underlying skeleton of flow transport [1, 2]. A significant factor influencing the surface transport of debris, oil and naturally floating material, however, is direct surface wind drag [3], which has yet to be accounted for in the LCS approach. We advance previous LCS work by directly incorporating wind effects into the analysis, and with application to ocean surface transport at the World Heritage Ningaloo coral reef in Western Australia, we demonstrate the significant consequences of accounting for windage. The waters surrounding Ningaloo are home to a burgeoning oil and gas industry and there is considerable importance in comprehending complex ocean surface transport in the region to support effective management and conservation.

References

[1] M. Mathur, G. Haller, T. Peacock, J.E. Ruppert-Felsot and H.L. Swinney, *Uncovering the Lagrangian skeleton of turbulence*, Phys. Rev. Lett. **98** (2007), 144502.

[2] T. Peacock and G. Haller, *Lagrangian Coherent Structures: The hidden skeleton of fluid flows*, Phys. Today **66** (2013), 41–47.

[3] A.J. Abscal, S. Castanedo, R. Medina, I.J. Losada and E. Alvarez-Fanjul, *Application of HF radar currents to oil spill modeling*, Mar. Pollut. Bull. **58** (2009) 238–248.

The dichotomy spectrum for random dynamical systems and pitchfork bifurcations with additive noise

Jeroen S. W. Lamb

(joint work with Mark Callaway, Doan Thai Son, Martin Rasmussen)

Despite its importance for applications, relatively little progress has been made towards the development of a bifurcation theory for random dynamical systems. Main contributions have been made by Ludwig Arnold and co-workers [2], distinguishing between *phenomenological* (P-) and a *dynamical* (D-) bifurcations. P-bifurcations refer to qualitative changes in the profile of stationary probability densities [16]. This concept carries substantial drawbacks such as providing reference only to static properties, and not being independent of the choice of coordinates. D-bifurcations refer to the bifurcation of a new invariant measure from a given invariant reference measure, in the sense of weak convergence, and are associated with a qualitative change in the Lyapunov spectrum. They have been studied mainly in the case of multiplicative noise [5, 8, 18], and numerically [1, 11].

In [6], we contribute to the bifurcation theory of random dynamical systems by shedding new light on the influential paper *Additive noise destroys a pitchfork bifurcation* by Crauel and Flandoli [7], in which the stochastic differential equation

$$\mathrm{d}x = \left(\alpha x - x^3\right)\mathrm{d}t + \sigma \mathrm{d}W_t\,, \tag{1}$$

with two-sided Wiener process $(W_t)_{t\in\mathbb{R}}$ on a probability space $(\Omega, \mathcal{F}, \mathbb{P})$, was studied. In the deterministic (noise-free) case, $\sigma = 0$, this system has a pitchfork bifurcation of equilibria: if $\alpha < 0$ there is one equilibrium ($x = 0$) which is globally attractive, and if $\alpha > 0$, the trivial equilibrium is repulsive and there are two additional attractive equilibria $\pm\sqrt{\alpha}$. [7] establish the following facts in the presence of noise, i.e. when $\sigma > 0$:

(i) For all $\alpha \in \mathbb{R}$, there is a unique globally attracting random fixed point $\{a_\alpha(\omega)\}_{\omega\in\Omega}$.
(ii) The Lyapunov exponent associated to $\{a_\alpha(\omega)\}_{\omega\in\Omega}$ is negative for all $\alpha \in \mathbb{R}$.

As a result, [7] concludes that the pitchfork bifurcation is destroyed by the additive noise. (This refers to the absence of D-bifurcation, as (1) admits a qualitative change P-bifurcation, see [2, p. 473].) However, we are inclined to argue that the pitchfork bifurcation is not destroyed by additive noise, on the basis of the following additional facts concerning the dynamics near the bifurcation point, that we obtain in this paper:

(i) The attracting random fixed point $\{a_\alpha(\omega)\}_{\omega\in\Omega}$ is uniformly attractive only if $\alpha < 0$.
(ii) At the bifurcation point there is a change in the practical observability of the Lyapunov exponent: when $\alpha < 0$ all finite-time Lyapunov exponents are negative, but when $\alpha > 0$ there is a positive probability to observe positive finite-time Lyapunov exponents, irrespectively of the length of time interval under consideration.
(iii) The bifurcation point $\alpha = 0$ is characterized by a qualitative change in the dichotomy spectrum associated to $\{a_\alpha(\omega)\}_{\omega\in\Omega}$. In addition, we show that the dichotomy spectrum is directly related to the observability range of the finite-time Lyapunov spectrum.

In light of these findings, we thus argue for the recognition of qualitative properties of the dichotomy spectrum as an additional indicator for bifurcations of random dynamical systems. Spectral studies of random dynamical systems have focused mainly on Lyapunov exponents [2, 9], but here we develop an alternative spectral theory based on exponential dichotomies that is related to the Sacker–Sell (or dichotomy) spectrum for nonautonomous differential equations. The original construction due to R.J. Sacker and G.R. Sell [17] requires a compact base set (which can be obtained, for instance, from an almost periodic differential equation). Alternative approaches to the dichotomy spectrum [3, 4, 13, 14, 15] hold in the general non-compact case, and we use similar techniques for the construction of the dichotomy spectrum by combining them with ergodic properties of the base

flow. We note that the relationship between the dichotomy spectrum and Lyapunov spectrum has also been explored in [10] in the special case that the base space of a random dynamical system is a compact metric space, but our setup does not require a topological structure of the base.

In analogy to the corresponding bifurcation theory for one-dimensional deterministic dynamical systems, we finally study whether the pitchfork bifurcation with additive noise can be characterized in terms of a breakdown of topologically equivalence. We recall that two random dynamical systems (θ, φ_1) and (θ, φ_2) are said to be topologically equivalent if there are families $\{h_\omega\}_{\omega\in\Omega}$ of homeomorphisms of the state space such that $\varphi_2(t, \omega, h_\omega(x)) = h_{\theta_t\omega}(\varphi_1(t, \omega, x))$, almost surely. We establish the following results for the stochastic differential equation (1):

(i) Throughout the bifurcation, i.e. for $|\alpha|$ sufficiently small, the resulting dynamics are topologically equivalent.
(ii) There does not exist a uniformly continuous topological conjugacy between the dynamics of cases with positive and negative parameter α.

These results lead us to propose the association of bifurcations of random dynamical systems with a breakdown of *uniform* topological equivalence, rather than the weaker form of general topological equivalence with no requirement on uniform continuity of the involved conjugacy. Note that uniformity of equivalence transformations plays an important role in the notion of equivalence for nonautonomous linear systems (i.e. in contrast to random systems, the base set of nonautonomous systems is not a probability but a topological space), see [12].

References

[1] L. Arnold, G. Bleckert and K.R. Schenk-Hoppé, *The stochastic Brusselator: parametric noise destroys Hopf bifurcation*, In *Stochastic Dynamics*, Springer, 1999.
[2] L. Arnold, *Random Dynamical Systems*, Springer, 1998.
[3] B. Aulbach and S. Siegmund, *The dichotomy spectrum for noninvertible systems of linear difference equations*, J. Difference Equ. Appl. **7** (2001), 895–913.
[4] A. Ben-Artzi and I. Gohberg, *Dichotomies of perturbed time varying systems and the power method*, Indiana Univ. Math. J. **42** (1993), 699–720.
[5] P.H. Baxendale, *A stochastic Hopf bifurcation*, Probab. Theory Related Fields **99** (1994), no. 4, 581–616.
[6] M. Callaway, Thai Son Doan, J.S.W. Lamb, M. Rasmussen, *The dichotomy spectrum for random dynamical systems and pitchfork bifurcations with additive noise*, preprint, available from `arxiv.org/abs/1310.6166`.
[7] H. Crauel and F. Flandoli, *Additive noise destroys a pitchfork bifurcation*, J. Dynam. Differ. Equ. **10** (1998), 259–274.
[8] H. Crauel, P. Imkeller and M. Steinkamp, *Bifurcation of one-dimensional stochastic differential equation*, In *Stochastic Dynamics*, Springer, 1999.
[9] N.D. Cong, *Topological Dynamics of Random Dynamical Systems*, Oxford University Press, 1997.
[10] R.A. Johnson, K.J. Palmer, and G.R. Sell, *Ergodic properties of linear dynamical systems*, SIAM J. Math. Anal. **18** (1987), 1–33.
[11] H. Keller and G. Ochs, *Numerical approximation of random attractors*, In *Stochastic Dynamics*, Springer, 1999.

[12] K.J. Palmer, *A characterization of exponential dichotomy in terms of topological equivalence*, J. Math. Anal. Appl. **69** (1979), 8–16.
[13] M. Rasmussen, *Dichotomy spectra and Morse decompositions of linear nonautonomous differential equations*, J. Differ. Equ. **246** (2009), 2242–2263.
[14] M. Rasmussen, *An alternative approach to Sacker-Sell spectral theory*, J. Difference Equ. Appl. **16** (2010), 227–242.
[15] S. Siegmund, *Dichotomy spectrum for nonautonomous differential equations*, J. Dynam. Differ. Equ. **14** (2002), 243–258.
[16] N. Sri Namachchivaya, *Stochastic bifurcation*, Applied Mathematics and Computation **38** (1990), 101–159.
[17] R.J. Sacker and G.R. Sell, *A spectral theory for linear differential systems*, J. Differ. Equ. **27** (1978), 320–358.
[18] B. Wang, *Stochastic bifurcation of pathwise random almost periodic and almost automorphic solutions for random dynamical systems*, submitted.

Comments on characterizing fluid flow mixing

Vered Rom-Kedar
(joint work with Ruty Mundel, Erick Fredj, Hezi Gildor)

Fluid mixing is a complex phenomenon - it involves a wide range of spatial and time scales in a variety of initial and boundary value problems. Nonetheless, some mathematical principles governing fluid mixing in real flows may be learned by considering simple toy models. One such principle, the emergence of dividing surfaces (the Lagrangian Coherent Structures, LCS [1]) as structures that govern fluid transport, much discussed in this workshop, was learned from studying transport in time periodic flows, where stable and unstable manifolds of selected hyperbolic periodic orbits provide the skeleton for fluid transport and mixing [2]. Three additional principles, learned from simple models, are pointed out as potentially useful lessons to be formulated and tested in real flows. 1) Homoclinic scales govern the nature of the transport by lobes [3]. 2) Weak three dimensional convection may simplify surface mixing by untangling the dividing surfaces [4]. 3) Resolving observable functions that distinguish between different coherent structures in the flow may help in substantial data reduction [6].

1) In time-periodic area preserving two dimensional flows, after proper rescaling of coordinates and time (roughly, rescale so that the averaged system has a homoclinic loop with size of order one and the velocity along the loop central part is also of order one), two important non-dimensional parameters appear - the amplitude of the oscillating component of the velocity and its frequency. The dependence of the tangle on these two parameters may be characterized in quite general settings. For example, the flux (lobes area divided by the period) dependence on the oscillating frequency is usually non-monotone and the homoclinic tangles at equi-flux frequencies have some specific structural differences [3, 5]. This phenomenon has to do with time and length scales that deform the dividing surfaces and is thus expected to be relevant to the LCS structure in finite time realizations in which the velocity field has a dominant period which is sufficiently small compared to the realization time.

2) The motion of surface particles is often modeled by time-periodic area preserving two dimensional flows, thus, their chaotic mixing is governed in such cases by homoclinic tangles. In many oceanographic applications, night convection makes the surface flow non-area preserving. Even though the vertical velocities are typically much smaller than the horizontal ones, such night convection typically lead to untangling the manifolds. The bi-directional flux associated with the homoclinic tangle is thus replaced by unidirectional flux from one region to the other. This phenomenon is observable at finite time realizations, and is controlled by appropriate comparison of the homoclinic scales of the oscillatory horizontal and vertical components [4]. Thus, similar phenomenon is expected to govern surface LCS geometry in realistic settings.

3) A new family of Lagrangian diagnostics is proposed [6] by which the spatial structure of extreme values of an observable are monitored. A specific form of it is suggested for characterizing mixing: the maximal extent of a trajectory in a given direction (MET). This new diagnostic enables the detection of coherent structures and their dynamics in two- (and potentially three-) dimensional unsteady flows in both bounded and open domains. Moreover, besides being an intuitive diagnostics, its computation seems much easier compared with all other Lagrangian diagnostics known to us. It provides new insights regarding the mixing properties on both short and long time scales and on both spatial plots and distribution diagrams. The usefulness and applicability of this diagnostic to two dimensional flows is demonstrated using toy models and a data set of surface currents from the Mediterranean Sea. It is shown that the size and position of coherent structures may be identified from the cumulative distribution function of the observable, thus leading to substantial data reduction.

References

[1] G. Haller and G. Yuan, *Lagrangian coherent structures and mixing in two-dimensional turbulence*, Physica D **147** (2000), 352–370.

[2] V. Rom-Kedar, A. Leonard and S. Wiggins, *An analytical study of transport, mixing and chaos in an unsteady vortical flow*, J. Fluid Mech. **214** (1990), 347–394.

[3] V. Rom-Kedar and A. Poje, *Universal properties of chaotic transport in the presence of diffusion*, Phys. Fluids **11** (1999), 2044–2057.

[4] R. Aharon, V. Rom-Kedar and H. Gildor, *When complexity leads to simplicity: Ocean surface mixing simplified by vertical convection*, Phys. Fluids **24** (2012), 056603.

[5] V. Rom-Kedar, *Frequency spanning homoclinic families*, Commun. Nonlinear Sci. Numer. Simulat. **8** (2003), 149–169.

[6] R. Mundel, E. Fredj, H. Gildor and V. Rom-Kedar, *New lagrangian diagnostics for characterizing fluid flow mixing*, submitted preprint, available from `arxiv.org/abs/1402.2604`.

Finite time curvature and a differential geometry perspective of shape coherence by nonhyperbolic splitting

Erik Bollt
(joint work with Tian Ma)

1. Introduction

Recently the notion of coherence has been pushed toward a more rigorous footing, and particularly within the recent advances of finite-time studies of nonautonomous dynamical systems. Here we recall shape coherent sets proved to correspond to slowly evolving curvature, for which tangency of finite time stable and unstable foliations plays a central role. Zero-angle curves, meaning non-hyperbolic splitting, describe boundaries of shape coherent sets. We show a Finite-Time Curvature evolution field (FTC) is particularly useful in identifying curves that correspond to persistent shape coherence.

2. Shape Coherence

We recently introduced a definition concerning coherence called shape coherent sets, motivated by an intuitive idea of sets that "hold together" through finite-time.

Definition (Finite Time Shape Coherence, [1])**.** The *shape coherence factor* α between two measurable nonempty sets A and B under a flow Φ_t after a finite time epoch $t \in 0:T$ is,

$$\alpha(A,B,T) \coloneqq \sup_{S(B)} \frac{m(S(B) \cap \Phi_T(A))}{m(B)},$$

where $S(B)$ is a group of transformations of rigid body motions of B.

We proved that angle of the finite-time stable and unstable foliations as defined,

$$\theta(z,t) \coloneqq \arccos \frac{\langle f_s^t(z), f_u^t(z)\rangle}{\|f_s^t(z)\|\|f_u^t(z)\|},$$

corresponds to level curves, and the zero level curves correspond to slowly evolving curvature. Furthermore, such curves can be proved to exist and constructed by the implicit function theorem. Finally considering a Finite-Time Curvature evolution field (FTC), by,

$$l_{\epsilon,v}(x) = \{\hat{x} = x + \epsilon s v, -1 < s < 1\},$$

then curvature growth at a point x over a time epoch is defined,

$$c_T(x) \coloneqq \lim_{\epsilon \to 0} \sup_{\|v\|=1} \kappa(\phi_T[l_{\epsilon,v}(x)]).$$

Level curves of this function corresponding a given low threshold can be shown to correspond to a given significant shape coherence, by use of theorem in [1]. See example of FTC in Fig. 1 and corresponding lowest values corresponding to outlining shape coherent sets of a Rossby wave.

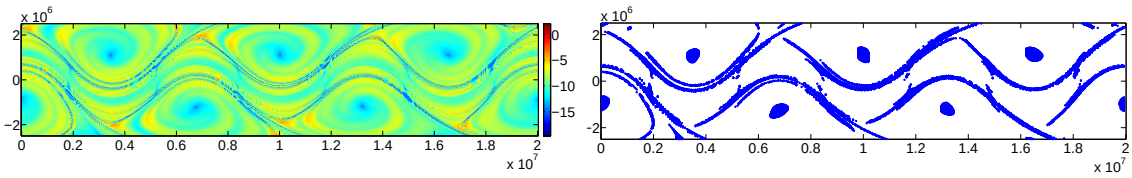

FIGURE 1. The FTC field of Rossby wave and a low threshold.

REFERENCES

[1] T. Ma and E. Bollt, *Differential Geometry Perspective of Shape Coherence and Curvature Evolution by Finite-Time Nonhyperbolic Splitting*, submitted.

Transport in microchannels: interaction between solenoidal and potential fields with noise

MASSIMILIANO GIONA
(joint work with Fabio Garofalo, Stefano Cerbelli)

1. INTRODUCTION

A critical analysis of the Literature focusing on transport phenomena and Brownian fluctuations in the presence of deterministic convective fields indicates the occurrence of a dichotomical splitting into two classes of subproblems, namely the interactions of thermal and molecular fluctuations either (i) with pure potential or (ii) pure solenoidal vector fields. This dichotomy can be attributed to a fallout of Hodge-Helmholtz decomposition of vector fields in two- and three-dimensional manifolds, where a generic smooth vector field $\mathbf{v}(\mathbf{x})$ can be expressed as a sum of a divergence-free component $\mathbf{v}_s(\mathbf{x})$, ($\nabla \cdot \mathbf{v}_s = 0$, $\mathbf{v}_s = \nabla \times \mathbf{A}$), and of an irrotational (potential) component $\mathbf{v}_p(\mathbf{x})$, ($\nabla \times \mathbf{v}_p = 0$, $\mathbf{v}_p = \nabla \phi$).

The "Middle-Earth" of vector fields possessing both non-vanishing divergence and curl remains substantially unexplored. In point of fact, the impetuous rise of microfluidics provides a relevant technological playground for studying transport phenomena in the presence of generic rotational and non-solenoidal velocity fields. This is due to the fact that magnetophoretic, dielectrophoretic and acoustophoretic flows in microchannels are characterized by the occurrence of a divergence-free channel flow, coupled for solute and particle transport to the potential velocity field accounting for the particle interaction with magnetic, electric, and pressure fields, respectively [1].

As a case study, we consider a simple problem, namely a two-dimensional acoustophoretic channel flow for micro-, nano-particle separation.

2. SETTING OF THE PROBLEM

In non-dimensional form, the Langevin equation for particle motion in a two-dimensional infinite channel (along the x-direction) in the presence of a steady

acoustophoretic potential, assuming negligible inertial effect (i.e. overdamped conditions), reads

$$dx(t) = u(y)\,dt + \sqrt{2\,\varepsilon}\,dw_x(t), \qquad dy(t) = \nu \sin(2\pi k y)\,dt + \sqrt{2\,\varepsilon}\,dw_y(t), \tag{1}$$

where $x \in (-\infty, \infty)$ is the axial coordinate along the channel, $y \in (0,1)$ is the transverse coordinate, Eq. (1) is equipped with reflecting conditions at $y = 0, 1$, i.e., at the channel walls, $u(y) = 6y(1-y)$ the Poiseuille flow, $\varepsilon = 1/Pe$ the reciprocal of the Péclet number, i.e., the dimensionless molecular diffusivity, $\sin(2\pi k y)$ the nondimensional acoustophoretic contribution $k = \ldots, -1, 1, 2, 3, \ldots$, and ν the dimensionless acoustophoretic intensity. The associated Fokker-Planck equation for the probability density function (pdf) $p(x, y, t)$ reads:

$$\partial_t p + u(y)\,\partial_x p + \nu\,\partial_y[\sin(2\pi k y)\,p] = \varepsilon\left(\partial_x^2 p + \partial_y^2 p\right).$$

where $(x, y) \in (-\infty, \infty) \times (0, 1)$, equipped with homogeneous Neumann conditions at the channel walls $\partial_y p|_{y=0,1} = 0$. In the long-term/large-distance limit, the marginal pdf $p_x(x,t) = \int_0^1 p(x, y, t)\,dy$ approaches the solution of a constant-coefficient equation $\partial_t p_x = -V_e \partial_x p_x + \varepsilon_e \partial_x^2 p$, where V_e and ε_e are respectively the effective velocity and the non-dimensional dispersion coefficient.

3. Results

From moment analysis [2, 3], we obtain that V_e and ε_e can be estimated analytically as follows [4]. Consider the transverse advection-diffusion operator:

$$\mathcal{L}_y[g(y)] = -\nu\,\partial_y(\sin(2\pi k y)\,g(y)) + \varepsilon\,\partial_y^2 g(y),$$

where $g \in L^2_{[0,1]}$, equipped with homogeneous Neumann boundary conditions, $\partial_y g|_{y=0,1}$. Let $\psi_0(y) \geq 0$ be the conservation eigenfunction, referred to as the *Frobenius eigenfunction* of $\mathcal{L}_y$, i.e. $\mathcal{L}_y[\psi_0(y)] = 0$, equipped with the above boundary conditions at $y = 0, 1$, and normalized to 1, $\int_0^1 \psi_0(y)\,dy = 1$. The effective velocity V_e is the average of $u(y)$ with respect to $\psi_0(y)$, i.e., $V_e = \int_0^1 u(y)\,\psi_0(y)\,dy$. The nondimensional effective dispersion coefficient ε_e is given by:

$$\varepsilon_e = \varepsilon + \int_0^1 \psi_0(y)\,[u(y) - V_e]\;b(y)dy = \varepsilon + \varepsilon \int_0^1 \psi_0(y)\,[\partial_y b(y)]^2\;dy,$$

where $b(y)$ is any solution of the elliptic problem (b-equation):

$$\mathcal{L}_y[\psi_0(y)\,b(y)] = \psi_0(y)\,[V_e - u(y)]\,,$$

equipped with homogeneous Neumann conditions $\partial_y b|_{y=0,1} = 0$.

From the analysis of the b-equation, it is possible to prove analytically that three dispersive regime can occur depending on k, i.e., on the number and symmetries of the stable nodes $y^*_{n,k} = (1 + 2n)/2k$, $n = 0, \ldots, k-1$, of the acoustophoretic potential:

- Case-I dispersion - It occurs if $u(y^*_{n,k}) = u^*$ for any $n = 0, \ldots, k-1$, and $\partial_y u(y)|_{y=y^*_{n,k}} = 0$ for any $n = 0, \ldots, k-1$, i.e., if all the stable nodes are characterized by the same axial velocity that in the neighbourhood

of each $y^*_{n,k}$ is locally quadratic. This is e.g. the case of $k = 1$. The qualitative property of Case-I dispersion is that ε_e vs Pe defines the graph of a unimodal function, with $\lim_{\varepsilon\to 0} \varepsilon_e/\varepsilon = \lim_{\varepsilon\to\infty} \varepsilon_e/\varepsilon = 1$.

- Case-II dispersion - It occurs if $u(y^*_{n,k}) = u^*$ for any $n = 0, \ldots, k-1$, and $Du_{\max} = \max_{n=0,\ldots,k-1} |\partial_y u(y)|_{y=y^*_{n,k}} > 0$, i.e., if all the stable nodes are characterized by the same axial velocity and at least at one node the axial velocity is locally linear (shear flow). This is e.g. the case of $k = 2$ or $k = -1$. In this case, it can be proved that $\lim_{\varepsilon\to 0} \varepsilon_e/\varepsilon = \kappa_D > 1$.
- Case-III dispersion - It occurs if $k > 1$ and

$$\Delta u^*_{\max} = \max_{m,n=0,\ldots,k-1} |u(y^*_{n,k}) - u(y^*_{m,k})| > 0,$$

i.e. in the generic case where there exist several (> 1) stable nodes possessing different axial velocities. This is the case for $k \geq 3$. It can be shown that $\varepsilon_e \sim \exp(\mu_k Pe)$, for $Pe = 1/\varepsilon \gg 1$, where $\mu_k = \nu/\pi k$.

4. Discussion

This simple model indicates that even elementary model flows (a 2-d parallel Poiseuille flow), coupled to particle transport can give rise to new and highly non trivial results.

The model considered in Case-III conditions is intrinsically characterized by the presence of "strong" transport barriers, represented by potential barriers between two neighbouring stable nodes. Transport across these barriers can occur solely via *stochastic tunneling*. Indeed, the phenomenon of stochastic tunneling is responsible of interesting transient anomalies, such as a *super-ballistic* scaling in the axial mean square displacement $\sigma^2_x(t) = \langle (x - \langle x \rangle)^2 \rangle \sim t^3$ as shown in Fig. 1. This phenomenon becomes more evident as ε decreases.

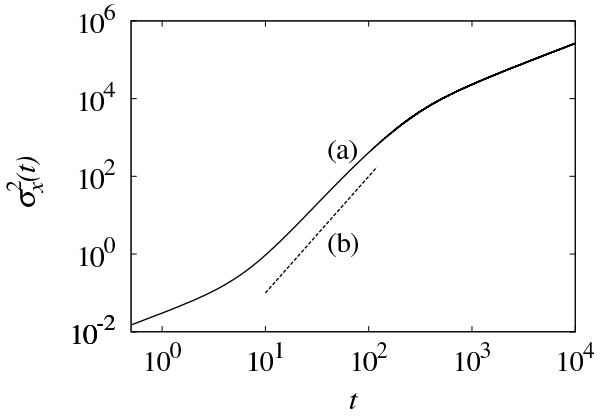

Figure 1. $\sigma^2_x(t)$ vs t at $k = 3$, $\nu = 1$, $\varepsilon = 1.5 \times 10^{-2}$. Line (a) Langevin simulations, line (b) scaling $\sigma^2_x(t) \sim t^3$.

A central issue that will be the focus of future investigation is the role of stochastic fluctuations (diffusion) in overcoming *strong* (potential) and *soft* (invariant manifolds) transport barriers in advecting-diffusing phenomena.

References

[1] H. Bruus, *Theoretical Microfluidics*, Oxford University Press, 2008.
[2] H. Brenner and D.A. Edwards, *Macrotransport Processes*, Butterworth, 1993.
[3] S. Cerbelli, M. Giona and F. Garofalo, *Quantifying dispersion of finite-sized particles in deterministic lateral displacement microflow separators through Brenner's macrotransport paradigm*, Microfl. Nanonfl. **15** (2013), 431–449.
[4] M. Giona, S. Cerbelli, F. Garofalo, Phys. Rev. E, submitted.

Reporter: Daniel Karrasch

Participants

Prof. Dr. Sanjeeva Balasuriya
School of Mathematical Sciences
University of Adelaide
Adelaide SA 5005
AUSTRALIA

Prof. Dr. Erik M. Bollt
Dept. of Mathematics & Computer Science
Clarkson University
Potsdam, NY 13699
UNITED STATES

Daniel F. Carlson
CNR-ISMAR
Istituto di Scienze Marine
Forte Sante Teresa
Pozzuolo di Lerici (SP)
Lerici (SP) 19032
ITALY

Prof. Dr. Michael Dellnitz
Institut für Mathematik
Universität Paderborn
33095 Paderborn
GERMANY

Prof. Dr. Charles R. Doering
Department of Mathematics
University of Michigan
530 Church Street
Ann Arbor, MI 48109-1043
UNITED STATES

Prof. Dr. Robert Ecke
Los Alamos National Laboratory
Center for Nonlinear Studies
Mail Stop B 258
Los Alamos, NM 87545
UNITED STATES

Prof. Dr. Bruno Eckhardt
Fachbereich Physik
Philipps-Universität Marburg
35032 Marburg
GERMANY

Mohammad Farazmand
Department of Mathematics
ETH Zürich, CLA, G 26
Tannenstrasse 3
8092 Zürich
SWITZERLAND

Margaux Filippi
Department of Mathematics
Massachusetts Institute of Technology
Cambridge, MA 02139-4307
UNITED STATES

Prof. Erick Fredj
Jerusalem College of Technology
Department of Computer Science
P. O. Box 16 031
Jerusalem 91160
ISRAEL

Prof. Dr. Gary Froyland
School of Mathematics and Statistics
University of New South Wales
Sydney NSW 2052
AUSTRALIA

Prof. Dr. Hezi Gildor
The Fredy & Nadine Herrmann Inst. of Earth Sc.
The Hebrew University
Edmond J. Safra Campus, Givat Ram
91904 Jerusalem
ISRAEL

Prof. Dr. Massimiliano Giona
Universita di Roma "La Sapienza"
Dipto. Ingegneria Chimica Materiali Ambiente
Via Eudossiana 18
00185 Roma
ITALY

Alireza Hadjighasem
Institute for Mechanical Systems
ETH Zürich, CLA, G 26
Tannenstrasse 3
8092 Zürich
SWITZERLAND

Prof. Dr. George Haller
Institute for Mechanical Systems
ETH Zürich
CLA Bldg. J 26
Tannenstrasse 3
8092 Zürich
SWITZERLAND

Prof. Dr. Emilio Hernandez-Garcia
Inst. de Fisica Interdiscipl. y Sistemas Complejos
IFISC CSIC - UIB
Campus Universitat Illes Balears
07122 Palma de Mallorca
SPAIN

Prof. Dr. Oliver Junge
Fakultät für Mathematik
Technische Universität München
85748 Garching bei München
GERMANY

Dr. Daniel Karrasch
Institute for Mechanical Systems
ETH Zürich
CLA G 27
Tannenstrasse 3
8092 Zürich
SWITZERLAND

Dr. Douglas H. Kelley
Department of Mechanical Engineering
University of Rochester
Rochester NY 14627
UNITED STATES

Dr. Jeroen Lamb
Department of Mathematics
Imperial College of Science, Technology and Medicine
London SW7 2AZ
UNITED KINGDOM

Dr. John R. Mahoney
University of California, Merced
5200 North Lake Road
Merced CA 95343
UNITED STATES

Prof. Dr. Ana Mancho
Instituto de Ciencias Matematicas, CSIC
Campus Cantoblanco, UAM
c/Nicolas Cabrera, 13-15
28049 Madrid
SPAIN

Prof. Dr. Kevin Mitchell
School of Natural Sciences
University of California, Merced
5200 North Lake Road
Merced, CA 95343
UNITED STATES

Prof. Dr. Nicholas Ouellette
Mechanical Engineering & Material Science
Yale University
P.O. Box 208286
New Haven CT 06520
UNITED STATES

Dr. Kathrin Padberg-Gehle
Technische Universität Dresden
Institut für Wissenschaftliches Rechnen
01062 Dresden
GERMANY

Prof. Dr. Tom Peacock
Dept. of Mechanical Engineering
Massachusetts Institute of Technology
Cambridge, MA 02139
UNITED STATES

Prof. Dr. Ronny Peikert
Department of Computer Science
ETH Zürich
Universitätsstr. 6
8092 Zürich
SWITZERLAND

Prof. Dr. Vered Rom-Kedar
Department of Computer Science and Applied Mathematics
The Weizmann Institute of Science
P.O.Box 26
Rehovot 76100
ISRAEL

Prof. Dr. Shane D. Ross
Virginia Tech
Dept. of Engineering Science & Mechanics
Norris Hall, Room 224
495 Old Turner St.
Blacksburg, VA 24061
UNITED STATES

Prof. Dr. Clarence Rowley
Department of Mechanical and Aerospace Engineering
Princeton University
Engineering Quad, Olden Street
Princeton, NJ 08544-5263
UNITED STATES

Prof. Dr. Irina Rypina
Woods Hole Oceanographic Institution
MS #21
266 Woods Hole Road
Woods Hole MA 02543
UNITED STATES

Prof. Dr. Stefan Siegmund
TU Dresden
Institute for Analysis & Center for Dynamics
01062 Dresden
GERMANY

Prof. Dr. Tom Solomon
Department of Physics and Astronomy
Bucknell University
Lewisburg, PA 17837
UNITED STATES

Prof. Dr. Michel Speetjens
Eindhoven University of Technology
Materials Technology
P.O. Box 513
5600 MB Eindhoven
NETHERLANDS

Prof. Dr. Mark Stremler
Dept. of Eng. Science & Mechanics (MC 0219)
Virginia Polytechnic Institute
Room 333P
495 Old Turner Street
Blacksburg, VA 24061
UNITED STATES

Prof. Dr. Wenbo Tang
School of Mathematics and Statistical Sciences
Arizona State University
Tempe, AZ 85287
UNITED STATES

Prof. Dr. Jean-Luc Thiffeault
Department of Mathematics
University of Wisconsin-Madison
480 Lincoln Drive
Madison, WI 53706-1388
UNITED STATES

Dr. Tino Weinkauf
Max-Planck-Institut für Informatik
Department 4: Computer Graphics
Campus E1 4
66123 Saarbrücken
GERMANY

Dr. Qinghai Zhang
Department of Mathematics
University of Utah
Salt Lake City, UT 84112-0090
UNITED STATES

Dr. Marton Zsugyel
MTA-BME
Water Resource Research Group
1111 Budapest
HUNGARY